Spectrochimica Acta Part A: Molecular and Biomolecular Spectroscopy 140 (2015) 111–131

Contents lists available at ScienceDirect

Spectrochimica Acta Part A: Molecular and Biomolecular Spectroscopy

journal homepage: www.elsevier.com/locate/saa

Polymer complexes. LX. Supramolecular coordination and structures of N(4-(acrylamido)-2-hydroxybenzoic acid) polymer complexes

M.M. Ghoneim [a], A.Z. El-Sonbati [b,*], A.A. El-Bindary [b], M.A. Diab [b], L.S. Serag [b,1]

[a] Chemistry Department, Faculty of Science, Tanta University, Tanta, Egypt
[b] Chemistry Department, Faculty of Science, Damietta University, Damietta, Egypt

HIGHLIGHTS

- Polymer complexes of N(4-(acrylamido)-2-hydroxybenzoic acid) (ABH) were synthesized and characterized.
- X-ray diffraction pattern show a mixture of polycrystalline and amorphous structure for polymer complexes.
- Molecular structures of ABH are optimized theoretically and quantum parameters are calculated.
- Thermodynamic parameters of the decomposition stages are evaluated and discussed.
- We found that the activation energy of PABH is greatly higher than its polymer complexes.

GRAPHICAL ABSTRACT

The XRD patterns of AB and ABH monomer powder forms.

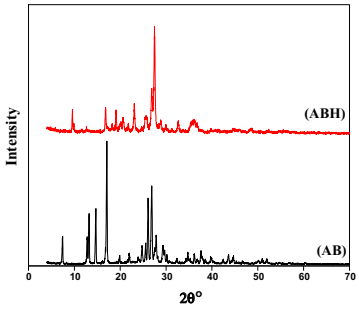

ARTICLE INFO

Article history:
Received 16 October 2014
Received in revised form 27 November 2014
Accepted 17 December 2014
Available online 27 December 2014

Keywords:
Polymer complexes
Thermogravimetric analysis
Thermodynamic parameters
Molecular structures
ESR
Quantum chemical parameters

ABSTRACT

A number of novel polymer complexes of various anions of copper(II), cobalt(II), nickel(II) and uranyl(II) with N(4-(acrylamido)-2-hydroxy benzoic acid) (ABH) have been synthesized and characterized by elemental analysis, IR, ^{1}H NMR, magnetic susceptibility measurements, electronic spin resonance, vibrational spectra and thermal analysis. The molecular structures of the ligand are optimized theoretically and the quantum chemical parameters are calculated. Tentative structures for the polymeric metal complexes due to their potential application are also suggested. The IR data exhibit the coordination of ONO_2/OAc/SO_4 with the metal ions in the polymeric metal complex. Vibrational spectra indicate coordination of carboxylate oxygen and phenolic OH of the ligand giving a MO_4 square planar chromophore. Ligand field ESR spectra support square planar geometry around Cu(II). The thermal decomposition of the polymer complexes were discussed in relation to structure, and the thermodynamic parameters of the decomposition stages were evaluated applying Coast–Redfern and Horowitz–Metzger methods.

Introduction

2-Hydroxybenzoic acid and its derivatives could present as a good model system for researching H-bonding and the effect of additional hydroxyl substitution in aromatic moieties. Extensive experimental and theoretical investigations have focused on elucidating the structures and normal vibrations of 2-hydroxybenzoic acid and its derivatives [1–3]. Karabacak et al. [1,2] were investigated 5-bromo-, 5-fluoro- and 5-chloro-2-hydroxybenzoic acid. They obtained 8 stable conformers for each molecule. The effect of the weak hydrogen bond between the dimers on geometry is

* Corresponding author. Tel.: +20 1060081581; fax: +20 572403868.
E-mail address: elsonbatisch@yahoo.com (A.Z. El-Sonbati).
[1] Abstracted from her M.Sc. Thesis.

http://dx.doi.org/10.1016/j.saa.2014.12.056
1386-1425/

investigated by comparison of the isolated-dimer and solid-state calculation by Takahashi et al. [3].

2-Hydroxybenzoic acid is widely used as plant growth regulators, as a preservative in food products, and in organic synthesis, antiseptic and anti-fungal agents. It has been shown to regulate a large variety of physiological processes in plants [4,5]. The structural features affect on the physico-chemical properties and on the bioactivity of these compounds. They have recently become attractive to experimentalists as well as theoreticians since their structures are of some biological significance particularly in phenolic anti-oxidants, medicine and enzyme chemistry [6–9].

Elvira and San Román [10] were synthesized the methacrylamide derivatives of 2-hydroxy-4-N-methacrylamidobenzoic acid (4-HMA) and 2-hydroxy-5-N-methacrylamidobenzoic acid (5-HMA). The monomers obtained present phenolic–OH and carboxylic functional groups in different positions of the side aromatic ring with respect to the methacrylamide group. The stereochemical configuration of polymers was analyzed for poly(4-HMA) and poly(5-HMA), the difference being explained in terms of the inter- and intramolecular interactions of the polar –OH and –COOH side groups through hydrogen bonding.

The present study describes the mechanism coordination behavior of novel monomer ABH with Cu(II), Co(II), Ni(II) and UO_2(II) ions. The structure of the studied polymer complexes is elucidated using elemental analyses, IR, ^{1}H NMR, solid reflectance, magnetic moment, ESR, molar conductance and thermal analyses measurements. The thermal decomposition and thermodynamic parameters of the polymer complexes were evaluated and discussed.

Experimental

Materials

All chemicals used were of the analytical reagent grade (AR), and of highest purity available. The chemicals used included acryloyl chloride (AC) (Aldrich Chemical Co., Inc.) was used without further purification. It was stored below −18 °C in a tightly glass-stoppered flask. 2,2′-Azobisisobutyronitrile (AIBN) (Aldrich Chemical Co., Inc.) was used as initiator for all polymerizations. It was purified by dissolving it in hot ethanol and filtering [11]. The solution was left to cool. The pure material was being collected by filtration and then dried. Metals of $CuCl_2$ and $Cu(NO_3)_2{\cdot}3H_2O$ (Sigma) and $Cu(OAc)_2{\cdot}H_2O$, $Co(OAc)_2{\cdot}4H_2O$, $Ni(OAc)_2{\cdot}4H_2O$ and $UO_2(NO_3)_2{\cdot}5H_2O$ (BDH). Organic solvents were spectroscopic pure from BDH Aldrich Chemical Co., Inc. included ethanol, benzene and dimethyl formamide.

Preparation of monomer and polymer

The amidation of 4-amino-2-hydroxybenzoic acid was performed with acryloyl chloride at 0 °C as described previously [12–14]. The crude product was crystallized from ethanol forming a gray powder of ABH monomer (Scheme 1). The yield is 75.23%, m.p. 170 °C. Analytical Calc. for C, 57.97; H, 4.35; N, 6.76%. Found: C, 57.77; H, 4.32; N, 6.66%.

Poly(N-4-acrylamido-2-hydroxybenzoic acid) (PABH) homopolymer was prepared by free radical initiation of ABH using (0.1 w/v) % AIBN as initiator and DMF as solvent and reflux for 6 h (Scheme 1). The polymer product was precipitated by pouring in distilled water and dried in a vacuum oven for several days at 40 °C.

Preparation of polymer complexes

In a typical preparation, a solution of ABH (0.01 mol) in dimethylformamide (DMF; 20 ml), the metal salts (0.01 mol) in DMF (25 ml), and (0.1 w/v%) AIBN as an initiator were used. The resulting mixture was heated at reflux for 8 h. The hot solution was precipitated by addition to a large excess of distilled water containing dilute HCl to remove the metal salts that were incorporated into the polymer complexes. The polymer complexes (**1**–**7**, see Table 1) were filtered, washed with water, and dried in a vacuum oven at 40 °C for several days.

Analysis and physical measurements

Microanalyses of carbon, hydrogen and nitrogen contents were performed on Automatic Analyzer CHNS Vario ELIII, Germany. The ^{1}H NMR spectra were carried out using Bruker WP 300 MHz using DMSO-d_6 as a solvent containing TMS as the internal standard. FT-IR spectra (KBr discs, 4000–400 cm^{-1}) were performed using Jasco-4100 spectrophotometer. Ultraviolet–Visible (UV–Vis) spectra of the compounds were recorded in DMF solution using a Unicom SP 8800 spectrophotometer. Thermal properties were investigated using Simultaneous Thermal Analyzer (TGA) STA 6000 with a scan rate 10 °C/min in air atmosphere from ambient temperatures to 800 °C. X-ray diffraction patterns of the powder form, is recorded on X-ray diffractometer with CuKα-radiation (λ = 1.540598 Å) in the range of diffraction angle ($2\theta^\circ$ = 4–70°). The applied voltage and the tube current are 40 kV and 30 mA, respectively. The molecular structures of the investigated compounds were optimized by HF method with 3-21G basis set. The molecules were built with the Perkin Elmer ChemBio Draw and optimized using Perkin Elmer ChemBio3D software [15,16]. ESR measurements of powdered samples were recorded at room temperature using an X-band spectrometer utilizing a 100 kHz magnetic field modulation with diphenylpicrylhydrazyl (DPPH) as a reference material. The conductance measurement was achieved using Sargent Welch scientific Co., Skokie, IL, USA.

Results and discussion

4-Acrylamido-2-hydroxybenzoic acid (ABH) monomer was prepared by amidation reaction of acryloyl chloride with 4-amino-2-hydroxybenzoic acid in benzene solvent with continuous stirring at 0 °C [13]. ABH monomer was polymerized by free radical polymerization by using 2,2′-azoisobutyronitrile (AIBN) as initiator.

All the polychelates are dark color solids. They are insoluble in common organic solvents. ABH-metal ion polymer complexes were prepared by the reaction of equimolar amounts of ABH monomer and metal salts using (0.1 w/v%) AIBN as initiator and DMF as solvent. The elemental analyses of all these polychelates indicate 1:1 and 1:2 (metal:ligand) stoichiometry (Table 1).

Theoretical study

Calculated energies and energy difference for all conformers of the 4-acrylamido-2-hydroxybenzoic acid (ABH), determined by HF method with 3-21G basis set. The geometrical structure scheme of all conformers is shown in Fig. 1. Stabilization energy of each conformer, the highest occupied molecular orbital energy (E_{HOMO}), the lowest unoccupied molecular orbital energy (E_{LUMO}) and the energy gap between HOMO and LUMO are summarized in Table 2. The lowest value of these stabilization energies showed that a stable conformer (C1). Intramolecular hydrogen bonds can be responsible for the geometry and the stability of a predominant conformation; the formation of hydrogen bonding between a hydroxyl group and COOH cause the structure of the conformer C1 to be the most stable conformer.

Comparison study is established between stable conformer of 4-amino-2-hydroxybenzoic acid (AB), ABH (C1) and ABH dimer

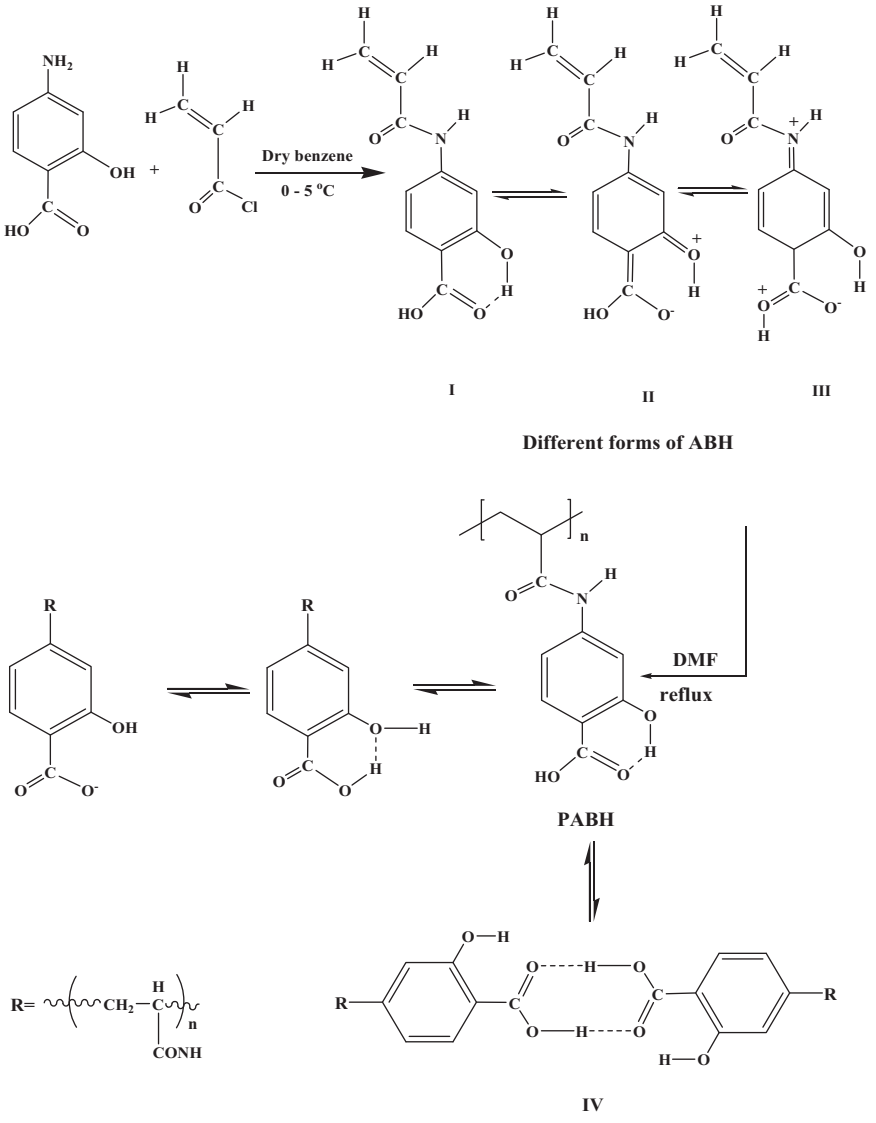

Scheme 1. The formation mechanism of ABH and PABH and intra- and inter-molecular hydrogen bond.

Table 1
Elemental analysis (C, H, N and M)[a] of polymer complexes (**1–7**) (for molecular structures see Fig. 5).

Compound[b]	$\mu_{eff.}$	Color	Experimental (calc.) (%)			
	B.M.		C	H	N	M
$[[UO_2(AB)_2]\cdot 2H_2O]_n$	dia.	Black	33.32	2.12	3.67	32.89
1			(33.43)	(2.23)	(3.9)	(33.15)
$[[Cu(AB)_2]\cdot 5/4H_2O]_n$	1.82	Deep brown	48.00	3.65	5.43	12.55
2			(48.19)	(3.72)	(5.62)	(12.76)
$[[Cu(AB)(ONO_2)(OH_2)]\cdot {}^3\!/_4H_2O]_n$	1.88	Brown	32.88	2.66	7.54	17.23
3			(33.06)	(2.76)	(7.71)	(17.5)
$[[Cu(AB)(OAc)]\cdot {}^1\!/_2H_2O]_n$	1.86	Deep brown	40.43	2.88	3.77	17.66
4			(40.51)	(3.09)	(3.94)	(17.87)
$[[Cu(ABH)(O_2SO_2)]\cdot {}^3\!/_4H_2O]_n$	1.84	Brown	31.46	2.28	3.55	16.47
5			(31.58)	(2.37)	(3.68)	(16.72)
$[[Co(AB)(OAc)(OH_2)]\cdot 2H_2O]_n$	4.61	Brown	37.87	3.33	3.43	15.33
6			(38.1)	(3.44)	(3.7)	(15.59)
$[[Ni(AB)(OAc)]\cdot 3H_2O]_n$	dia.	Brown	38.00	2.77	3.54	15.32
7			(38.13)	(2.91)	(3.71)	(15.54)

[a] The excellent agreement between calculated and experimental data supports the assignment suggested in the present work.
[b] L is the anion of ABH as given in Scheme 1, insoluble in water, but partially soluble in ethanol and completely soluble in DMF.

structures (Fig. 2). We found that, AB has higher stabilization energy than ABH and its dimer structure, so AB is less stable than ABH and ABH dimer (Table 3). Intermolecular hydrogen bond which is formed in ABH dimer showed lower stabilization energy than monomeric form (ABH). So, ABH dimer is more stable compared to ABH.

Molecular structure (HOMO & LUMO) is shown in Fig. 3 for all conformers. Also HOMO & LUMO of AB, ABH (C1) and its dimer structure are presented in Fig. 4. The HOMO–LUMO energy gap, ΔE, which is an important stability index, is applied to develop theoretical models for explaining the structure and conformation barriers in many molecular systems. The smaller is the value of ΔE, the more is the reactivity of the compound has [17–19]. The calculated quantum chemical parameters are given for all conformers in Table 2 and for AB, ABH and ABH dimer in Table 3, respectively. Additional parameters such as separation energies, ΔE, absolute electronegativities, χ, chemical potentials, Pi, absolute hardness, η, absolute softness, σ, global electrophilicity, ω [20,21], global softness, S, and additional electronic charge, ΔN_{max}, have been calculated according to the following equations [22]:

$$\Delta E = E_{LUMO} - E_{HOMO} \tag{1}$$

$$\chi = \frac{-(E_{HOMO} + E_{LUMO})}{2} \tag{2}$$

$$\eta = \frac{E_{LUMO} - E_{HOMO}}{2} \tag{3}$$

$$\sigma = \frac{1}{\eta} \tag{4}$$

$$Pi = -\chi \tag{5}$$

$$S = \frac{1}{2\eta} \tag{6}$$

$$\omega = \frac{Pi^2}{2\eta} \tag{7}$$

$$\Delta N_{max} = -\frac{Pi}{\eta} \tag{8}$$

The predicted bond lengths and bond angles for most stable conformer AB, ABH (C1) and ABH dimer are tabulated in Tables 4 and 5.

In the ring part, the C–C bond lengths of the benzene ring for AB are observed in the range 1.34–1.353 Å. The C=O bond lengths in the carboxylic acid group conform to the average values are tabulated for an aromatic carboxylic acid in which C=O is 1.212 Å and C–O is 1.358 Å. The NH_2 showed identical value of N–H bond lengths (1.049 Å). ABH showed nearly values to AB bond lengths,

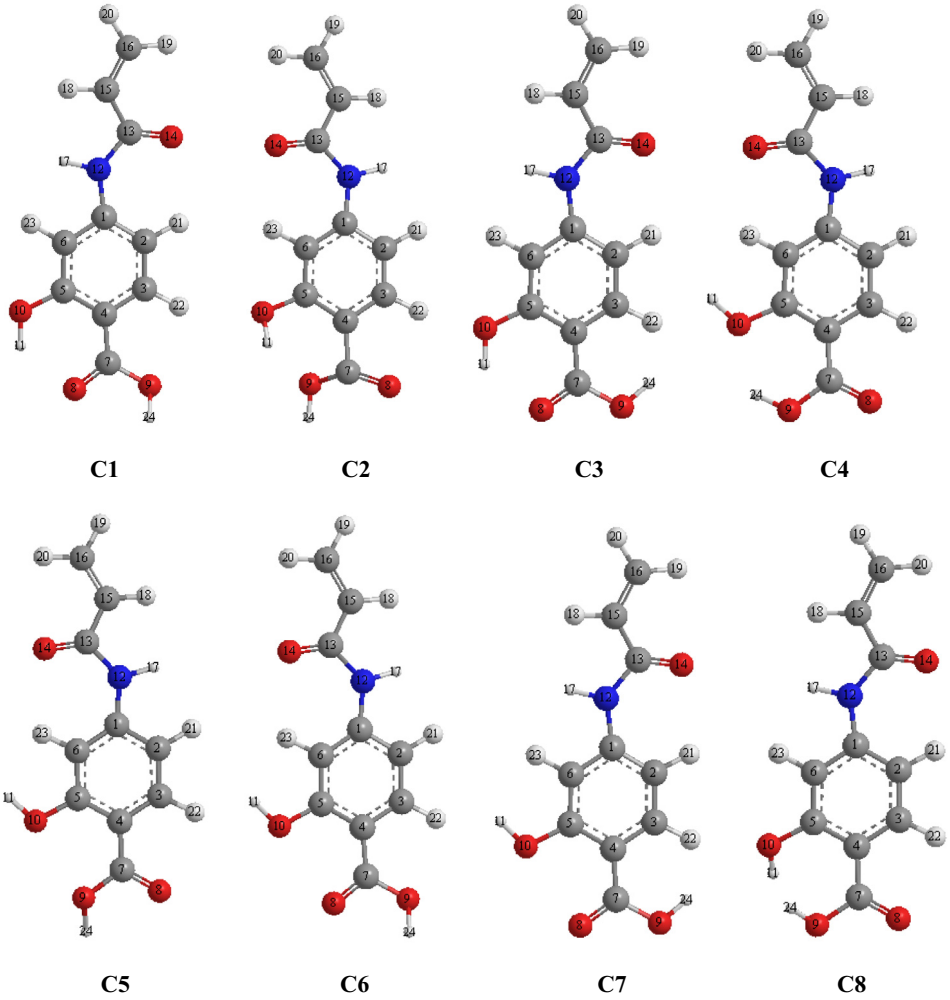

Fig. 1. Molecular structure with atomic numbering for all conformers of ABH.

Table 2
Stabilization energy, HOMO, LUMO and other additional parameters of all ABH Conformers.

Compound	E_{HOMO} (a.u.)	E_{LUMO} (a.u.)	ΔE (a.u.)	χ (a.u.)	η (a.u.)	σ (a.u.)$^{-1}$	Pi (a.u.)	S (a.u.)$^{-1}$	ω (a.u.)	ΔN_{max}
1	−0.3481	−0.1701	0.1780	0.2590	0.0890	11.223	−0.2590	5.6117	0.3755	2.903
2	−0.4158	−0.1676	0.2482	0.2917	0.1241	8.0580	−0.2917	4.0290	0.3430	2.351
3	−0.4184	−0.1694	0.2490	0.2939	0.1245	8.0305	−0.2939	4.0152	0.3469	2.360
4	−0.4174	−0.1710	0.2464	0.2942	0.1232	8.1158	−0.2942	4.0579	0.3513	2.388
5	−0.4176	−0.1730	0.2446	0.2953	0.1223	8.1766	−0.2953	4.0883	0.3565	2.414
6	−0.4180	−0.1711	0.2469	0.2945	0.12345	8.1001	−0.2945	4.0500	0.3514	2.386
7	−0.4193	−0.1698	0.2494	0.2945	0.12474	8.0163	−0.294	4.0081	0.3477	2.361
8	−0.4167	−0.1710	0.2457	0.2938	0.1228	8.1400	−0.2938	4.0700	0.3515	2.392

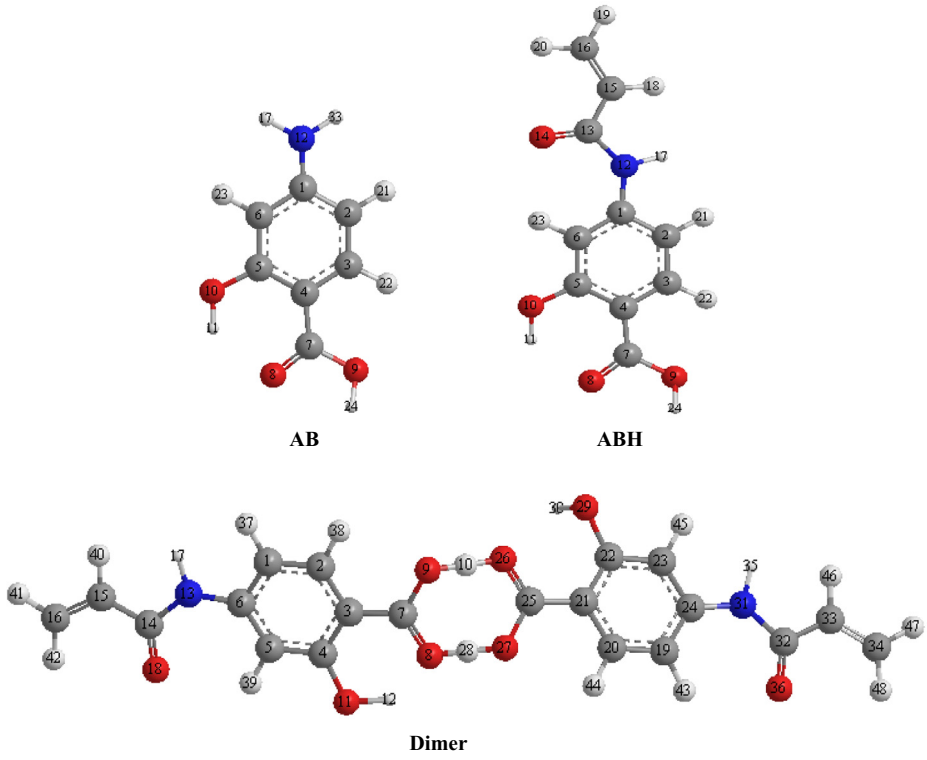

Fig. 2. Molecular structure with atomic numbering for AB, ABH and ABH dimer.

Table 3
Stabilization energy, HOMO, LUMO and other additional parameters of AB, ABH and its dimer.

Compound	E_{HOMO} (a.u.)	E_{LUMO} (a.u.)	ΔE (a.u.)	χ (a.u.)	η (a.u.)	σ (a.u.)$^{-1}$	Pi (a.u.)	S (a.u.)$^{-1}$	ω (a.u.)	ΔN_{max}
AB	−0.425	−0.095	0.330	0.260	0.165	6.052	−0.260	3.0259	0.2048	1.574
ABH	−0.372	−0.179	0.194	0.276	0.097	10.337	−0.276	5.048	0.393	2.849
Dimer	−0.347	−0.173	0.174	0.260	0.086	11.510	−0.260	5.7554	0.3907	2.999

while showed a remarkable change in NH bond length of ABH due to bonding with acryloyl molecule. In ABH, N–H bond length is 1.01 and N–C bond length is 1.365.

Bond angle C5–C4–C7 is smaller than C3–C4–C7 because of interaction between the carboxyl acid (COOH) and hydroxyl (OH) group of AB and ABH (Fig. 2). These results are in agreement with literatures [1–3]. The torsional angles of AB (C5–C4–C7–O9 and C3–C4–C7–O8 are 179.992° and 179.997°, respectively) and ABH (C5–C4–C7–O9 and C3–C4–C7–O8 are 178.8° and 179.3°, respectively). The tilt angles are calculated 180°. The dihedral angles are nearly the same among the all conformers.

The geometric structure of ABH dimer is also calculated (Fig. 2). Stabilization energy lowest value of dimer showed higher stability than ABH. Intermolecular hydrogen bonds can be responsible for the geometry and the stability of a predominant conformation; the formation of hydrogen bonding between two molecules via a hydroxyl group and –COOH cause the structure of the dimer to be the most stable conformer. The intermolecular hydrogen bonds are almost linear (the O–H...O angle equals 179.4°) and their length is 2.063 Å. The intramolecular hydrogen bonds between the hydroxyl groups and the oxygen atoms of the carbonyl groups are strongly bent (the O–H...O angle equals 164.7°) and the O...O distance is 2.056 Å [23].

Composition and structure of polymer complexes

The solid polymer complexes of Cu(II) and UO_2(II) ions with ABH monomer are subjected to elemental analyses, IR, ^{1}H NMR, solid reflectance, magnetic studies, molar conductance and ther-

mal analyses to identify their tentative formulae in a trial to elucidate their molecular structure.

The data of elemental analysis as given in Table 1 denote that three types of complexes were formed. For the first case the ligand behave as a monobasic and not contains anion (complex without chloride anions) (1M:2L molar ratio, Fig. 5(A)).

$$UO_2(NO_3)_2 \cdot 5H_2O + ABH \rightarrow [[UO_2(AB)_2] \cdot 2H_2O]_n$$

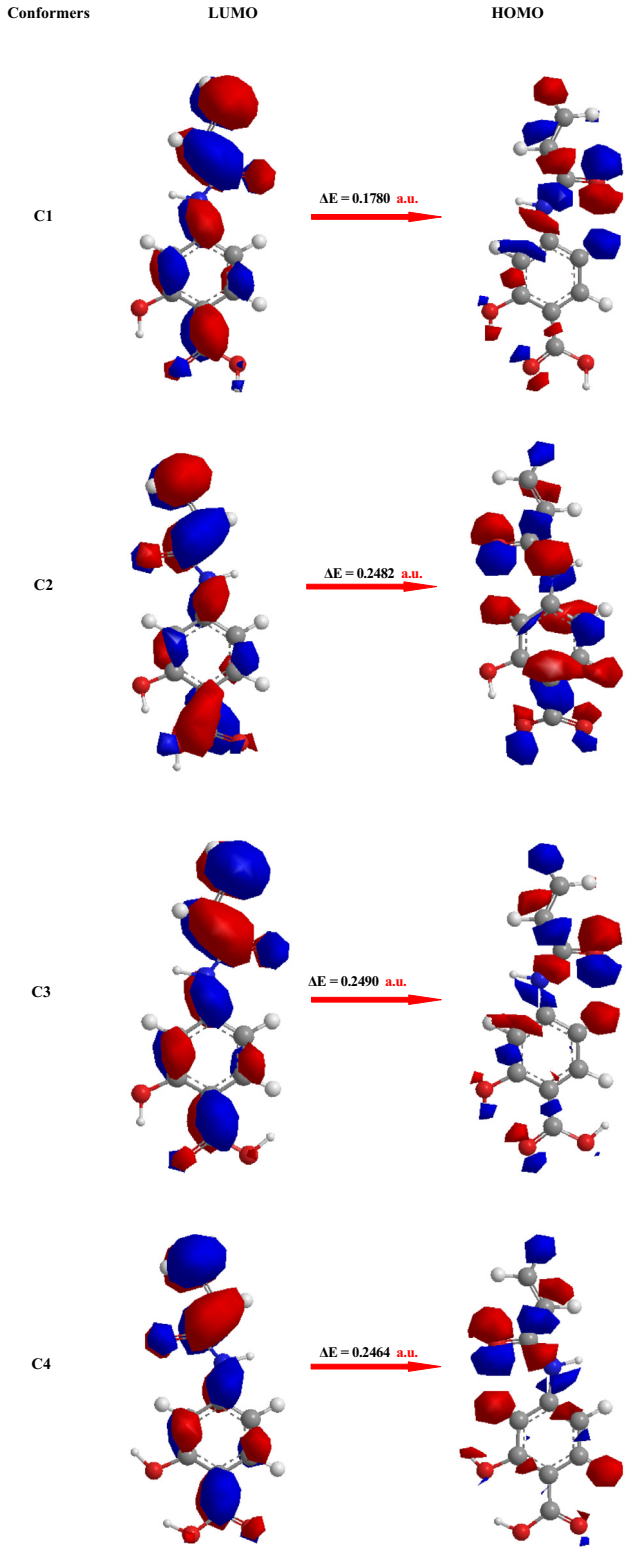

Fig. 3. Molecular structure HOMO and LUMO for ABH conformers.

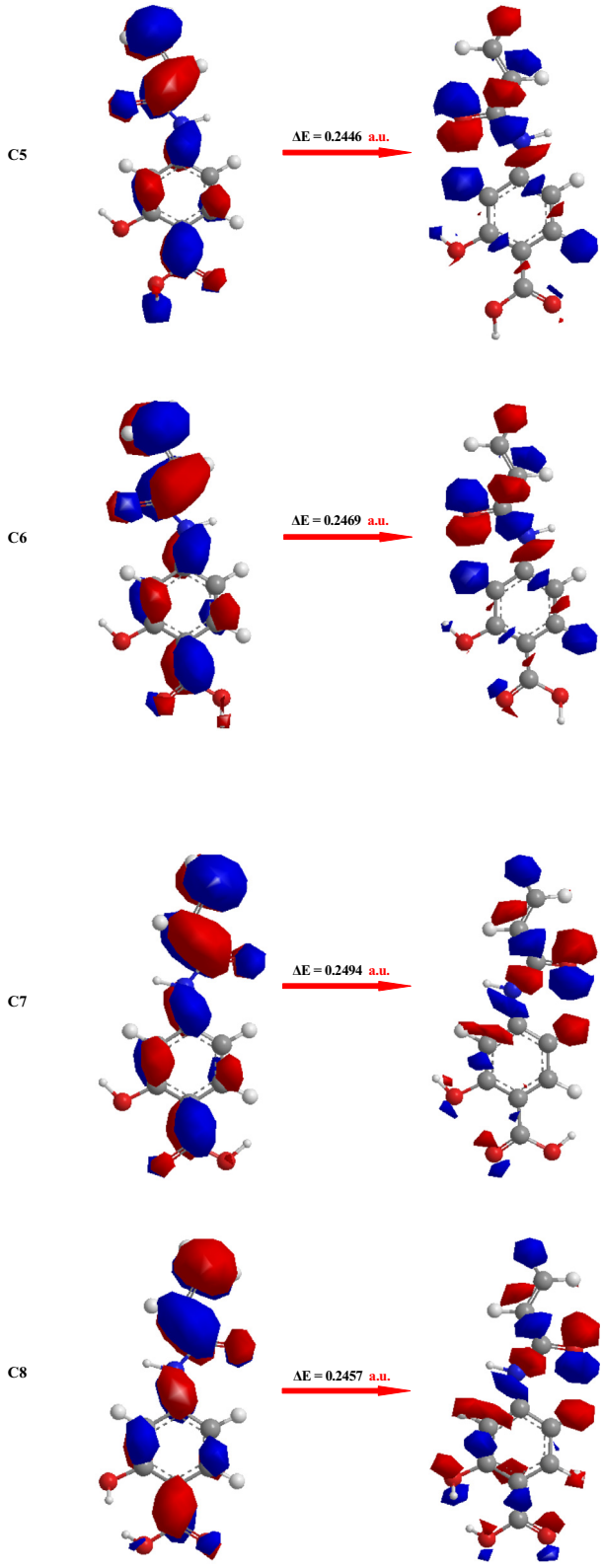

Fig. 3 (*continued*)

$$CuCl_2 + ABH \rightarrow [[Cu(AB)_2] \cdot \frac{5}{4}H_2O]_n$$

For the second case the ligand behave as a monobasic and contains one anion (complexes with half equivalent anions) (1M:1L molar ratio, as shown in Fig. 5(B and C)).

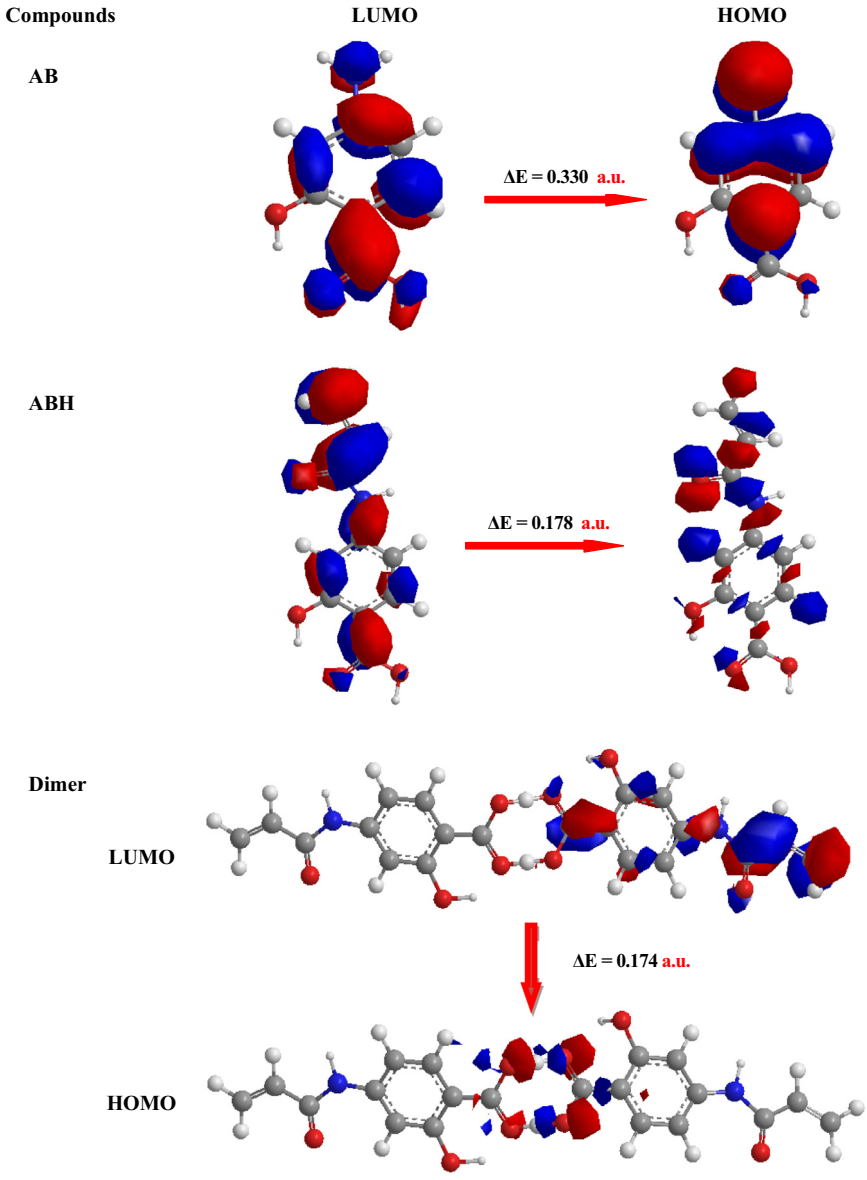

Fig. 4. Molecular structures HOMO and LUMO for AB, ABH (C1) and ABH dimer.

$$Cu(NO_3)_2 \cdot 3H_2O + ABH \rightarrow \left[[Cu(AB)(ONO_2)(OH_2)] \cdot \frac{3}{4}H_2O\right]_n$$

$$Cu(OAc)_2 \cdot H_2O + ABH \rightarrow \left[[Cu(AB)(OAc)] \cdot \frac{1}{2}H_2O\right]_n$$

$$Co(OAc)_2 \cdot 4H_2O + ABH \rightarrow [[Cu(AB)(OAc)(OH_2)] \cdot 2H_2O]_n$$

$$Ni(OAc)_2 \cdot 4H_2O + ABH \rightarrow [[Ni(AB)(OAc)] \cdot 3H_2O]_n$$

For the third case the ligand behave as a neutral and contains anion (complex with equivalent anion) (1M:1L molar ratio, Fig. 5D)

$$CuSO_4 \cdot 5H_2O + ABH \rightarrow \left[[Cu(ABH)(O_2SO_2)] \cdot \frac{3}{4}H_2O\right]_n$$

Where AB = deprotonated ABH.

The molar conductance values for the polymer complexes (**1–7**) (10^{-3} M) are determined in DMF and these values are found to be a low value which indicates the non-ionic nature of these polymer complexes and there is no counter ion present outside the coordination sphere of polymer complexes [24].

The number of water molecules varies according to the nature of the metals. Thus the results of elemental analysis clarify, that three types of bonding are formed between the M^{2+} ions and the ligand under study, those with covalent, ionic and partially ionic and covalent bonds.

All the polymer complexes have high melting point, denoting a strong bonding between the ligand and metal ions. It is interesting to point out that, the data of elemental analysis are in satisfactory agreement with the expected formula which gives support for the suggested composition.

Infrared spectra

The IR spectra of ABH ligand and all these polychelate resemble each other in general appearance. However there is a noticeable difference in certain vibrational frequencies.

Examination of IR spectrum of the ABH shows a medium broad band around 3400–3100 cm^{-1} which may be assigned to OH of

Table 4
Bond lengths for AB, ABH and its dimer.

Bond lengths (Å)					
AB		ABH		Intermolecular hydrogen bond (ABH Dimer)	
O(9)–H(10)	0.971	O(9)–H(24)	0.971	O(9)–H(10)	1.010
C(5)–H(18)	1.104	C(6)–H(23)	1.098	H(10)–O(26)	1.075
C(1)–H(16)	1.103	C(3)–H(22)	1.102	O(27)–H(28)	0.991
C(2)–H(17)	1.103	C(2)–H(21)	1.104	H(28)–O(8)	1.072
O(11)–H(12)	0.971	O(10)–H(11)	1.0	O(11)–H(12)	0.995
C(4)–O(11)	1.363	C(5)–O(10)	1.379	H(12)–O(8)	1.061
C(7)–O(9)	1.358	C(7)–O(9)	1.349	O(29)–H(39)	1.003
C(7)–O(8)	1.212	C(7)–O(8)	1.229	O(26)–H(39)	1.073
C(3)–C(7)	1.368	C(4)–C(7)	1.366		
C(6)–C(1)	1.339	C(6)–C(1)	1.346		
C(5)–C(6)	1.34	C(5)–C(6)	1.345		
C(4)–C(5)	1.346	C(4)–C(5)	1.35		
C(3)–C(4)	1.353	C(3)–C(4)	1.339		
C(2)–C(3)	1.348	C(2)–C(3)	1.342		
C(1)–C(2)	1.341	C(1)–C(2)	1.348		
N(13)–H(15)	1.049	N(12)–H(17)	1.01		
N(13)–H(14)	1.049	N(12)–C(13)	1.365		
C(6)–N(13)	1.268	N(12)–C(1)	1.35		
		C(13)–C(15)	1.36		
		C(13)–O(14)	1.206		
		C(15)–C(16)	1.342		
		C(16)–H(20)	1.1		
		C(16)–H(19)	1.102		
		C(15)–H(18)	1.105		

Table 5
Bond angles for AB, ABH and its dimer.

Bond angles (°)					
AB		ABH		Intermolecular hydrogen bond (ABH Dimer)	
H(15)–N(13)–C(6)	120.281	C(1)–N(12)–H(17)	109.793	O(26)–H(10)–O(9)	176.730
H(14)–N(13)–C(6)	120.161	C(1)–N(12)–C(13)	133.388	O(8)–H(28)–O(27)	179.427
H(15)–N(13)–H(14)	119.558	H(17)–N(12)–C(13)	116.819	O(11)–H(12)–O(8)	164.782
O(9)–C(7)–O(8)	113.465	O(9)–C(7)–O(8)	119.333	O(29)–H(39)–O(26)	164.113
O(9)–C(7)–C(3)	121.977	O(9)–C(7)–C(4)	125.455		
O(8)–C(7)–C(3)	124.558	O(8)–C(7)–C(4)	115.212		
C(4)–C(3)–C(7)	118.119	C(7)–C(4)–C(5)	118.337		
C(2)–C(3)–C(7)	122.862	C(7)–C(4)–C(3)	123.144		
C(1)–C(6)–N(13)	120.422	N(12)–C(1)–C(6)	126.721		
C(5)–C(6)–N(13)	120.593	N(12)–C(1)–C(2)	115.026		
		H(20)–C(16)–C(15)	122.966		
		C(15)–C(13)–O(14)	124.552		
		C(15)–C(13)–N(12)	111.542		
		O(14)–C(13)–N(12)	123.905		
Torsional angles (°)					
C(2)–C(3)–C(7)–O(8)	179.992	C(5)–C(4)–C(7)–O(9)	178.807		
C(4)–C(3)–C(7)–O(9)	179.997	C(3)–C(4)–C(7)–O(8)	179.382		

phenolic, carboxylic O–H and amide –N–H stretching vibration [25]. This observed region may be due to mixing of intramolecular and intermolecular hydrogen bonding due to N–H and O–H groups (Scheme 1(I and IV)). Well resolved sharp band around 3300 cm^{-1} observed in the spectra of all polymer metal complexes indicates the presence of an N–H/O–H group indicative of participation of carboxylic OH group in metal bonding. The spectrum of ligand ABH shows strong bands at 1690 and 1660 cm^{-1} which may be attributed to carbonyl stretching frequencies due to aromatic carboxylic and amide groups, respectively.

All the polymer metal complexes show the absence of a band at 1690 cm^{-1} and shift in the band of the amide around 1660 cm^{-1} to around 1650–30 cm^{-1}. It is quite possible that the band due to carboxylic carbonyl group would have been involved in coordination with metal ion while amide carbonyl group may not be participating in direct metal bonding. However, all the polymer metal complexes reveal the presence of two bands around 1600 and 1460 cm^{-1}. This may be due to the carboxylate ion [26]. It is well established that the band around 1600 cm^{-1} is due to symmetric stretching and that of 1460 cm^{-1} is due to anti-symmetric stretching vibrations of the carboxylate ion [27]. The frequency difference $[\Delta\upsilon = \upsilon_{as}(COO^-) - \upsilon_s(COO^-)]$ can be used as an indication of the binding mode of the carboxylate [27]. If $\Delta\upsilon$ is greater than 200 cm^{-1}, the group is probably bound in a monodentate way, as was observed for the polymeric complexes reported herein.

A strong band at 1280 cm^{-1} in the spectrum of ligand may be due to hydrogen bonded O–H in plane bonding vibration. All the polymer metal complexes show this band shifted to 1250 cm^{-1} which may be due to –O–M suggesting coordination through the carboxylic oxygen [28]. These two bands are either slightly shifted to lower frequencies or remained decreased markedly in intensity. This indicates that the carboxylate group participated in complex formation with the metal ions [28].

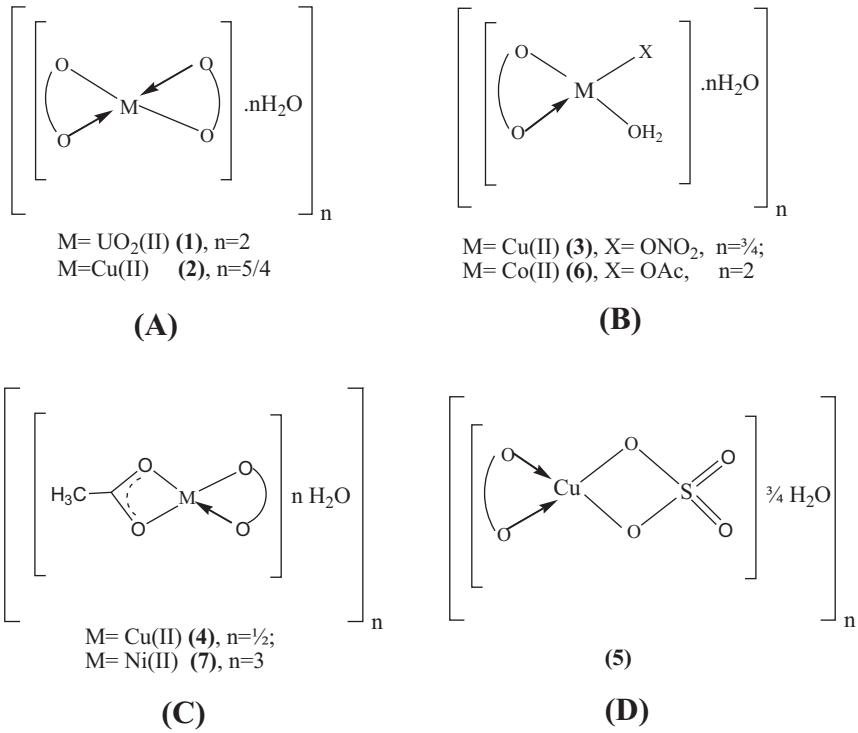

Fig. 5. Structure of polymer complexes.

Participation of the phenolic and carboxylic OH groups is also confirmed by the appearance of new bands in the complexes is the 465–445 cm^{-1} regions which is consistent with the υ(M–O) stretching vibration [29] as suggested by Soliman and Mohamed [25]. In the IR spectrum of the polymer complex containing nitrate as the gegenion, the band observed at 275 cm^{-1} can be assigned to υ(Cu–ONO_2), consistent with the bands at 255 cm^{-1} reported earlier for Cu–ONO_2 in metal complex [30]. Moreover, in the nitrato polymer complex of ABH, two strong bands at 1285 and 1407 cm^{-1} corresponding to υ_1 and υ_4 modes of nitrato groups with a separation of 122 cm^{-1} indicate the presence of a terminally bonded monodentate nitrate group [31]. The IR spectrum of polymer complex (**5**) contains strong bands at 1000, 1115, 1206 cm^{-1} due to υ_3, 955 cm^{-1} due to υ_1 and 465 cm^{-1} due to υ_2, and these can be assigned to a bridging bidentate sulfato group [31]. In the acetate polymer complex (**6**) the peaks are observed at 1561 cm^{-1} υ(C=O) and 1388 cm^{-1} υ(C–O); the difference in the main two peaks, i.e. 173 cm^{-1} suggests that the acetate ions are coordinated to the metal ion in monodentate fashion [31,32].

In the polymer complexes (**4** & **7**), the bands which are observed near 1530 and 1435 cm^{-1} attributed to υ_{as}(OCO) and υ_s(OCO) of the acetate group, respectively, indicate asymmetric bidentate coordination of this group ($\Delta\upsilon(OCO) = \upsilon_{as}(OCO) - \upsilon_s(OCO) <$ 100 cm^{-1}) [33].

The IR spectrum of the uranium polymer complex (**1**) exhibits two bands at 942 and 822 cm^{-1} which are assignable to υ_{as}(O=U=O) and υ_s(O=U=O) modes, respectively. This observation indicates that the linearity of the O=U=O group is maintained in the complex [34]. The force constant (*f*) for the υ_{as}(O=U=O) mode was calculated for polymer complex (**1**) by the following the method of McGlynn et al. [35]. It was found to be 7.34 mdyne/Å, and agrees well with the force constant values of similar dioxouranium(VI) complexes [36]. From this work, the U–O bond distance R_{U-O} was calculated by using Jone's equation [37], $R = 1.08f^{-1/3} + 1.17$, where *f* is the force constant for the υ_{as}(O=U=O). It was found to be 1.72 Å, and this is in the usual range (1.60–1.92 Å) observed for dioxouranium(IV) complexes [36].

The existence of water of hydration and/or water of coordination in the spectra of all the polymer metal complexes render it difficult to get conclusion from the phenolic group of the ligand, which would be overlapped by those of the water molecules. The participation of the phenolic group is further confirmed by clarifying the effect of chelation on the υ(C–O) stretching vibration. The shift of the υ(C–O) of phenolic group, from 1280 cm^{-1} in the free ligand to 1270–1255 cm^{-1} in the polymer metal complexes formation [10,34]. Also the participation of the OH group is apparent from the shift in position of the δ(OH) in-plane bending from 1395 cm^{-1} in the free ligand to 1390–1375 cm^{-1} in the polymer metal complexes [38].

The presence of water molecule in the polymer metal complexes are assisted by the appearance of a broad band within the range 3450–3300 cm^{-1}, which is attributed to υ(OH_2) of the water molecules associated with the polymer complex formation. Also a bending vibration of the water molecules, δ(OH_2), is found in the range 960–915 cm^{-1}. The other bending vibration of the water molecules, δ(OH_2), is usually around 1600 cm^{-1} which always interferes with the skeleton vibration of the benzene ring (C=C vibration).

^{1}H NMR spectra

The ^{1}H NMR spectrum of PABH homopolymer was recorded in DMSO-d_6 solution using TMS as internal standard, includes six resonances at 10.80, 7.57, 7.28, 3.20, 2.53 and 2.10 ppm relative to TMS which may be assigned to the COOH, CONH, aromatic protons, OH phenolic, vinylic –CH– and –CH_2 protons, respectively. There is a weak peak at 3.25 ppm due to the water proton. On addition of D_2O the intensities of NH, OH and COOH protons significantly decreases. The peaks at (10.80, 3.20 and 7.57 ppm), which are due to the exchangeable hydrogen-bonded carboxyl/hydroxyl/amine (COOH/OH/NH) proton, disappear upon exchange with

D_2O and can be associated with the COOH/OH/NH protons involved in intramolecular hydrogen bonding indicating the involvement of the COOH group in chelation through displacement of the COOH proton.

In the ^1H NMR spectrum of polymer complex (**1**), the signal for the proton of COOH group disappeared, suggesting the participation of COOH proton to the metal center in the formation of COO-M and the proton of phenolic OH group were shifted towards down field, due to the coordination of phenolic oxygen with metal and a significant shifting in all the peaks was observed which confirm the formation of polymer metal complex. The peak of aromatic protons became broad due to the intramolecular interaction towards the metal ion and variation in the π-electron density around the protons.

X-ray diffraction

The X-ray diffraction patterns (XRD) of AB, ABH monomer and its complexes in powder forms are shown in Figs. 6 and 7, respectively. The XRD patterns of the AB and ABH monomer powder forms are polycrystalline with different structure and various degree of crystallinity (Fig. 6). The XRD pattern for polymer complexes (**1** & **2**) indicates a mixture of polycrystals and amorphous structure (Fig. 7 (**1** & **2**)). While the XRD patterns for all other copper polymer complexes (Fig. 7 (**3**–**5**)) are completely amorphous. The average crystallite size (D) can be determined using by Scherrer equation [39–41]:

$$D = \frac{0.9\lambda}{\beta_{1/2}\cos\theta} \quad (9)$$

The equation uses the reference peak width at angle (θ), where λ is wavelength of X-ray radiation (1.541874 Å) and $\beta_{1/2}$ is the width at half maximum of the reference diffraction peak measured in radians. The dislocation density, δ, is the number of dislocation lines per unit area of the crystal. The value of δ is related to the average particle diameter (D) by the relation [40]:

$$\delta = \frac{1}{D^2} \quad (10)$$

The values of D are 418 and 270 nm for AB and ABH monomer, respectively. The values of δ are 5.72×10^{-6} and 1.37×10^{-5} for AB and ABH monomer, respectively.

TGA analysis

The thermal behavior of PABH homopolymer and its polymer complexes (**1**–**7**) were investigated using thermogravimetric analysis (TGA). TGA curves of all compounds are shown in Fig. 8. Weight loss percentage in each stage of PABH homopolymer and its polymer complexes (**1**–**7**) is presented in Table 6. It can be seen clearly that the mass losses obtained from the TG curves and that calculated for the corresponding molecule or molecules as well as the final decomposition product are in good agreement for all of the decomposition steps. PABH homopolymer shows two decomposition steps [42,43], the first stage occur in the temperature range 170–185 °C is attributed to decarboxylation mechanism (Found 29.95% and calc. 28.07%). The second stage in the temperature range 185–255 °C corresponding to combustion of a part of the monomer (C_6H_4N) (Found 43.73%; calc. 42.99%) and at higher temperature 300–605 °C, loss of acrylaldehyde molecule (C_3H_3O) (Found 26.32%; calc. 26.57%) [42]. All polymer complexes showed TG curves in the temperature range ~30 to 120 °C loss of outer water molecules. The second stage is related to loss of CO_2 gas or coordinated water molecule. The third stage is attributed to loss of a part of the monomer. The final weight losses are due to the decomposition of the rest of the monomer leaving metal oxides residue (Table 6).

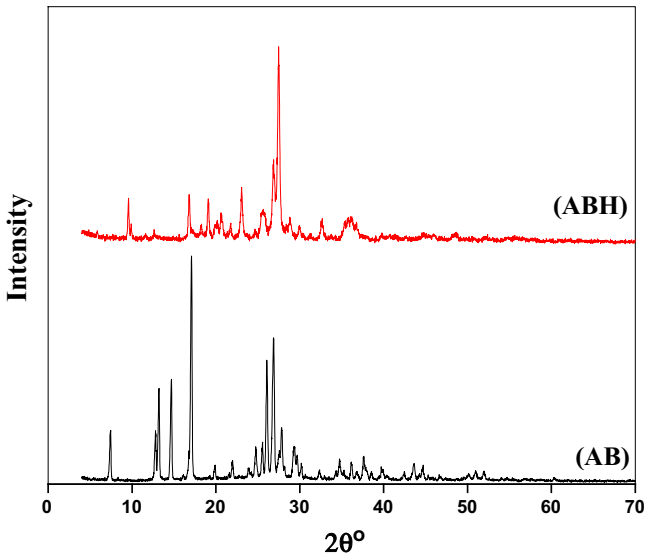

Fig. 6. The XRD patterns of AB and ABH monomer powder forms.

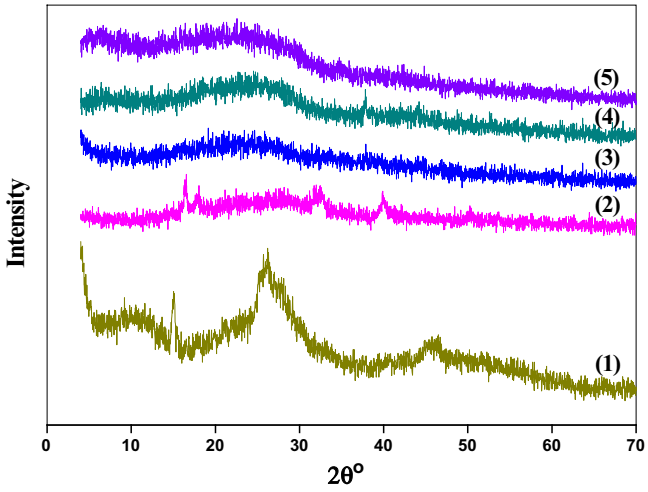

Fig. 7. The XRD patterns of polymer complexes powder forms (**1**–**5**).

The TGA is used for the determination of rates of degradation of PABH homopolymer and its polymer complexes. The rate constant of the thermal decomposition was plotted according to the Arrhenius relationship [44,45]:

$$\ln K^* = \ln Å - E^*/RT$$

where K^* is the rate constant of the thermal degradation, Å is a pre exponential constant, E^* the thermal activation energies of decomposition, R is a gas constant (= 8.314 J K^{-1} mol^{-1}) and T is the absolute temperature. The activation energies of decomposition (E^*) are calculated from the slope of the straight line obtained from the plot ln K^* versus $1/T$. The values of E^* are listed in Table 7. It is clear that, the activation energy of PABH homopolymer is greatly higher than its polymer complexes (**1**–**7**). Therefore, PABH is more stable than the polymer complexes (**1**–**7**), which may be attributed to steric hindrance. The relation between E^* and representative Pascal constants of complexes (**3**–**5**) is shown in Fig. 9. It is observed that the activation energy (E^*) value of the formed polymer complexes increases in the order NO_3^- > OAc^- > SO_4^{2-}. Our results are also in

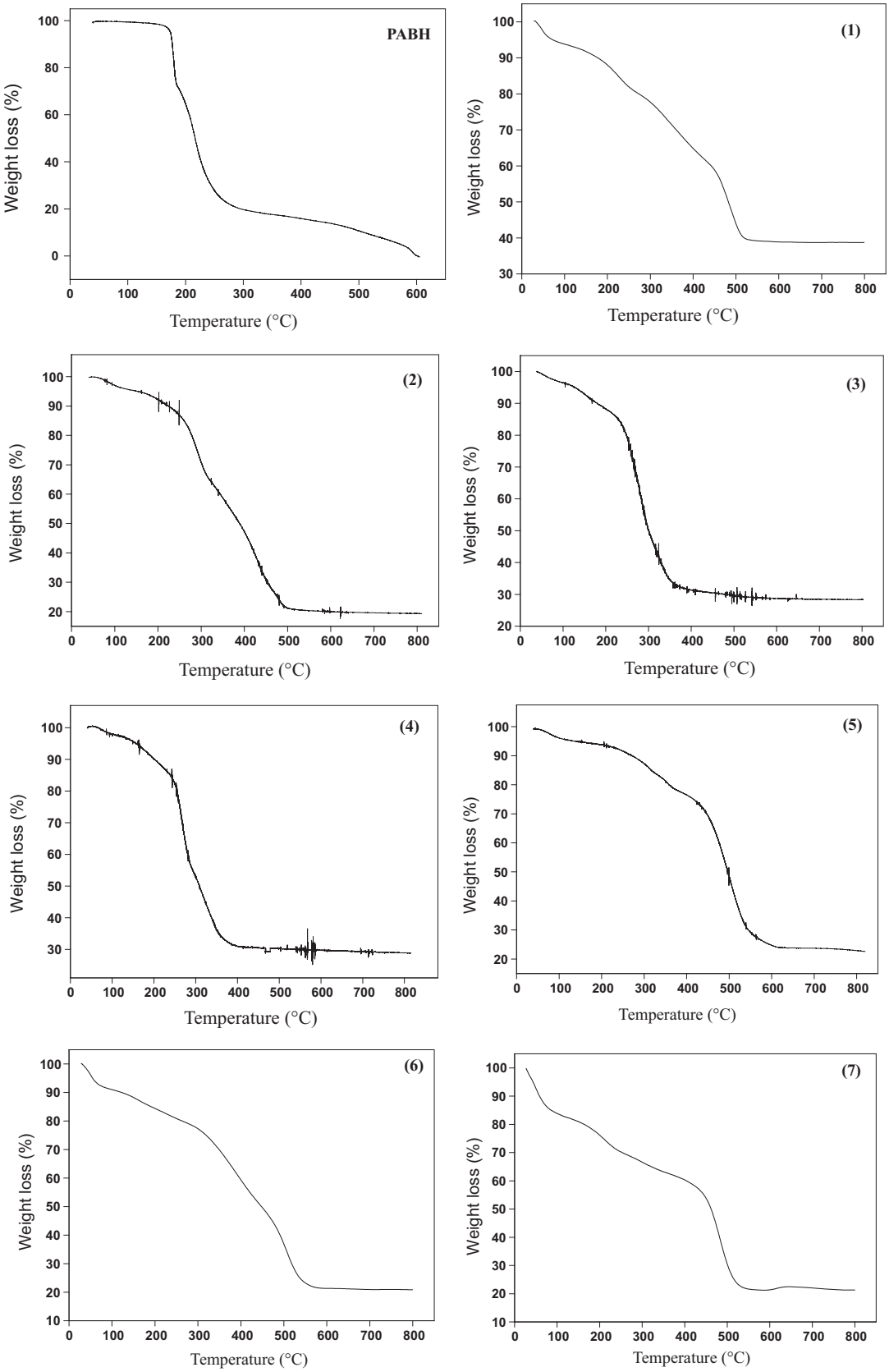

Fig. 8. TGA diagrams of PABH homopolymer and its polymer complexes (**1**–**7**).

Table 6
Thermal data of PABH homopolymer and its polymer complexes (**1–7**).

Compound[a]	Temperature range (°C)	TG weight loss % Found (Calc.)	Assignments
PABH	170–185	29.95 (28.07)	CO_2
	185–255	43.73 (42.99)	C_6H_4N
	300–605	26.32 (26.57)	C_3H_3O
1	40–80	5.01 (5.62)	$2H_2O$
	80–245	12.22 (12.00)	$2CO_2$
	245–660	45.12 (43.36)	$C_{18}H_{16}N_2O_4$
	>800	37.60 (38.61)	UO_2
2	40–133	4.55 (4.52)	$1¼H_2O$
	133–303	28.54 (28.30)	$CO_2 + H_2O + NH_3$
	303–442	35.87 (35.34)	$C_{13}H_6N$
	442–492	9.97 (11.0)	C_3H_3O
	>800	21.07 (21.07)	CuO + 2C
3	40–104	3.73 (3.72)	$¾H_2O$
	104–181	6.40 (4.95)	H_2O
	181–301	40.06 (41.59)	$CO_2 + C_6H_5ON$
	301–340	12.67 (14.12)	NO_2
	>800	37.14 (37.05)	C_3H_3O + CuO
4	40–95	2.35 (2.53)	$½H_2O$
	95–178	6.46 (5.06)	H_2O
	178–281	35.72 (35.54)	$CO_2 + C_6H_4$
	281–345	20.20 (20.40)	$C_5H_5O_2N$
	>800	37.04 (36.29)	C_3H_3O + CuO
5	40–105	3.67 (3.55)	$¾H_2O$
	105–354	16.39 (16.84)	SO_2
	354–560	52.44 (52.87)	$CO_2 + C_7H_9NO_3$
	>800	27.50 (27.22)	CuO + 2C
6	30–90	8.79 (9.53)	$2H_2O$
	90–320	16.50 (16.40)	$H_2O + CO_2$
	320–580	58.18(54.24)	$CH_3COO + C_9H_8NO$
	>800	21.53 (19.83)	CoO
7	30–85	14.92 (14.29)	$3H_2O$
	85–430	27.50 (27.27)	$CO_2 + CH_3COO$
	430–700	36.56 (38.66)	$C_9\ H_8NO$
	>800	21.79 (19.78)	NiO

[a] The number corresponds to that used in Table 1.

agreement with the respective positions of these anions as given in the representative Pascal constants [46].

Kinetic studies

The thermodynamic activation parameters of decomposition processes of complexes namely activation energy (E_a), enthalpy (ΔH^*), entropy (ΔS^*), and Gibbs free energy change of the decomposition (ΔG^*) are evaluated graphically by employing the Coast–Redfern [47] and Horowitz–Metzger [48] methods.

Coast–Redfern equation

The Coast–Redfern equation, which is a typical integral method, can represent as:

$$\int_0^a \frac{dx}{(1-\alpha)^n} = \frac{A}{\varphi}\int_{T_1}^{T_2} \exp\left(-\frac{E_a}{RT}\right)dt \tag{11}$$

For convenience of integration, the lower limit T_1 usually taken as zero. This equation on integration gives:

$$\ln\left[-\frac{\ln(1-\alpha)}{T^2}\right] = -\frac{E_a}{RT} + \ln\left[\frac{AR}{\varphi E_a}\right] \tag{12}$$

A plot of left-hand side (LHS) against $1/T$ was drawn (Fig. 10). E_a is the energy of activation in J mol^{-1} and calculated from the slop and A in (s^{-1}) from the intercept value. The entropy of activation ΔS^* in (J K^{-1} mol^{-1}) calculated by using the equation:

$$\Delta S^* = 2.303\left[\log\left(\frac{Ah}{k_B T_s}\right)\right]R \tag{13}$$

Table 7
Arrhenius relationship activation energy for PABH homopolymer and its polymer complexes (**1–7**).

Compound[a]	E^* (kJ/mol)
PABH	341.46
1	36.87
2	47.58
3	79.81
4	77.58
5	35.70
6	41.93
7	34.46

[a] The number corresponds to that used in Table 1.

where k_B is the Boltzmann constant, h is the Plank's constant and T_s is the TG peak temperature.

Horowitz–Metzger equation

The Horowitz–Metzger equation is an illustrative of the approximation methods. These authors derived the relation:

$$\log\left[\frac{1-(1-\alpha)^{1-n}}{1-n}\right] = \frac{E_a\theta}{2.303RT_s^2} \quad \text{for } n\neq 1 \tag{14}$$

when $n = 1$, the LHS of equation 14 would be $\log[-\log(1-\alpha)]$ (Fig. 11). For a first order kinetic process, the Horowitz–Metzger equation may write in the form:

$$\log\left[\log\left(\frac{W_\alpha}{W\gamma}\right)\right] = \frac{E\theta}{2.303RT_s^2} - \log 2.303 \tag{15}$$

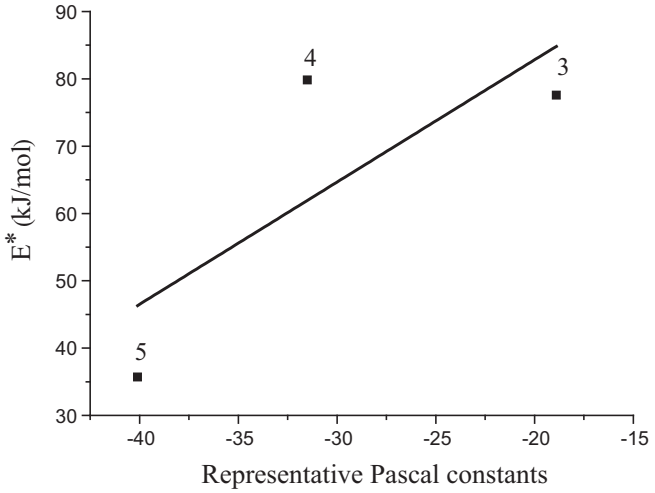

Fig. 9. The relation between E^* and representative Pascal constants of polymer complexes (**3**–**5**).

where $\theta = T - T_s$, $W_\gamma = W_\alpha - W$, W_α = mass loss at the completion reaction; W = mass loss up to time t. The plot of log [log (W_α/W_γ)] vs. θ was drawn and found to be linear from the slope of which E_a was calculated. The pre-exponential factor, A, calculated from equation:

$$\frac{E_a}{RT_s^2} = \frac{A}{\left[\varphi \exp\left(-\frac{E_a}{RT_s}\right)\right]} \tag{16}$$

The entropy of activation, ΔS^*, is calculated from Eq. (13). The enthalpy activation, ΔH^*, and Gibbs free energy, ΔG^*, calculated from:

$$\Delta H^* = E_a - RT \tag{17}$$

$$\Delta G^* = \Delta H^* - T\Delta S^* \tag{18}$$

The calculated values of E_a, A, ΔS^*, ΔH^* and ΔG^* for the decomposition steps for PABH and its polymer complexes are summarized in Table 8. The kinetic data obtained from the two methods are comparable and can be considered in good agreement with each other.

Electronic spectra and magnetic moments

Elemental analyses, IR and molar conductivity data were used to prove the stoichiometry and formulation of the polymer complexes. A square planar geometry were assumed for all copper(II), nickel(II) and tetrahedral geometry was found for cobalt(II) polymer complexes based on their magnetic data and spectral studies.

The Ni(II) polymer complex show diamagnetic properties and the electronic spectrum of this complex show bands at 16,110 and 21,930 cm^{-1} which are assigned as $^1A_{1g} \rightarrow {}^1A_{2g}$ and $^1A_{1g} \rightarrow {}^1B_{1g}$ transitions, respectively. The electronic spectrum of Co(II) polymer complex show absorption band at 13,690 cm^{-1} assignable to $^4A_2(F) \rightarrow {}^4T_1(P)$, which is characteristic value for the tetrahedral Co(II) complex. The magnetic moment of Co(II) is 4.61 B.M. suggesting four coordinate tetrahedral geometry.

The $\mu_{eff.}$ values of the Cu(II) polymeric complexes are normal within the range reported for one unpaired electron in a tetrahedral or square planar geometry (Table 1). It is impossible to differentiate between these two geometries on the basis of electronic spectra. Instead, it may be distinguished on the basis of ESR spectra.

In the electronic spectra of the ligand and its polymeric metal complexes, there are wide range bands were observed due to either the $\pi \rightarrow \pi^*$ and $n \rightarrow \pi^*$ of C=O chronopher or charge-transfer transition arising from π-electron interactions between the metal and ligand, which involved either a metal-to-ligand or ligand-to-metal electron transfer [49]. The electronic spectra of the free ligand in DMF showed strong absorption bands in the region 35,450–23,800, that could be attributed to the $\pi \rightarrow \pi^*$ and $n \rightarrow \pi^*$ transitions in the benzene ring or C=O groups for free ligand. The absorption bands in the ligand changed a bit in intensity and remained slightly changed for metal polymeric complexes. The absorption shift and intensity change in the spectra of the metal polymeric complexes most likely originated from the metallation, increased the conjugation and delocalization of the whole electronic system and resulted in the energy change of the $\pi \rightarrow \pi^*$ and $n \rightarrow \pi^*$ transitions of the conjugated chromophore [50].

The electronic spectra of polymer complexes revealed a broad bands in the region 18,300–18,600 and 19,800–20,200 cm^{-1} assignable respectively to the transition $^2B_{1g} \rightarrow {}^2B_{1g}$ and $^2B_{1g} \rightarrow {}^2E_g$, state and is the measure of the difference between in-plane and axial fields. Since the in-plane field is constant in all present cases, the change in the position of the bands would be due to the axial field only. In these copper(II) polymer complexes, the spectral bands are found to be sensitive to the nature of the anion X, and shift to higher energy in the order $NO_3^- > OAc^- > SO_4^{2-}$. Thus, these spectral data indicating the possibility of a square planar environment around the Cu(II) ion [51], where the ligand is bidentate and the axial position are occupied by the anions and/or water (Fig. 5).

Electron spin resonance

The ESR spectra of a variety of copper(II) complexes have been measured in order to investigate the bonding character of copper–ligand bonds in the complexes. The bonding parameters showing the degree of covalency for the bonds have been estimated from the magnetic parameters, namely, the g and A values, determined from their ESR spectra [44,51]. Little attention has been paid to the interesting and important problem of binding some correlation between the degree of covalency thus obtained and the chemical and physical properties of the complexes or their ligand molecules themselves. However, it is not easy to do this because of the fact that the ESR of the complexes is substantially concerned with only the antibonding orbitals associated with the copper atom.

The ESR spectra of polymer complexes (**2**–**5**) are characteristic of a d^9, configuration and having an axial shape with $g_{\|} > g_{\perp}$ characteristic of polymer complexes with $^2B_{1g}(d_{x2\text{-}y2})$ ground state. The g-values suggest a square planar geometry [52]. The ESR parameters are presented in Table 9. The average g values were calculated according to:

$$g_{av.} = 1/3[g_{\|} + 2g_{\perp}]$$

and give values in the range 2.120–2.127. The ESR data are reported in Table 9. The $g_{av.}$ values for the polymer complexes studies follow the order:

$$\left[[Cu(AB)(OAc)] \cdot \frac{1}{2}H_2O\right]_n > \left[[Cu(ABH)(O_2SO_2)] \cdot \frac{3}{4}H_2O\right]_n > \left[[Cu(AB)_2] \cdot \frac{5}{4}H_2O\right]_n > \left[[Cu(AB)(ONO_2)(OH_2)] \cdot \frac{3}{4}H_2O\right]_n.$$

In axial symmetry, the g values are correlated by the expression = $(g_{\|} - 2)/(g_{\perp} - 2)$, which reflects the exchange interaction between copper(II) centers in the solid polycrystalline complex

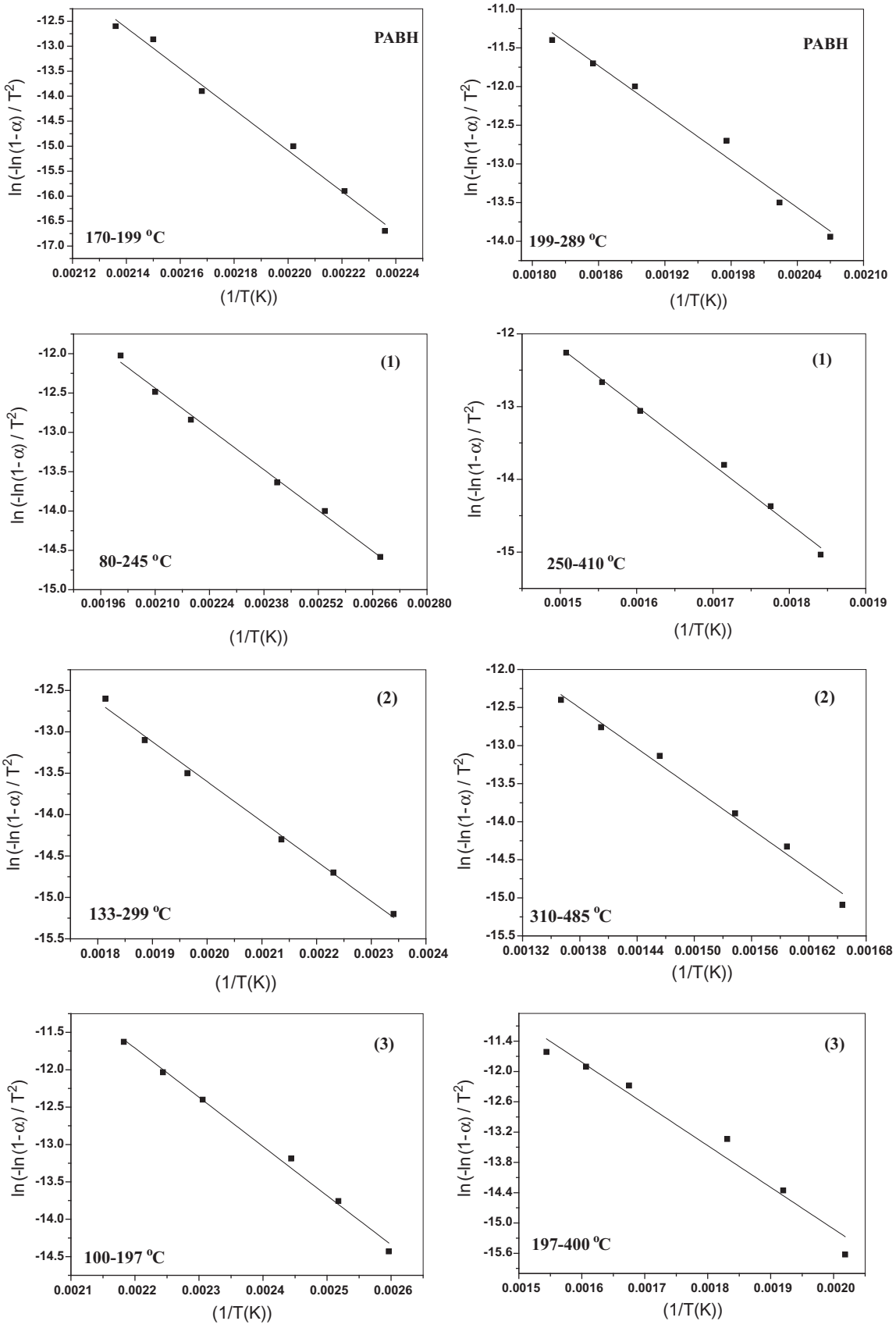

Fig. 10. Coats–Redfern (CR) of PABH homopolymer and its polymer complexes (**1**–**7**).

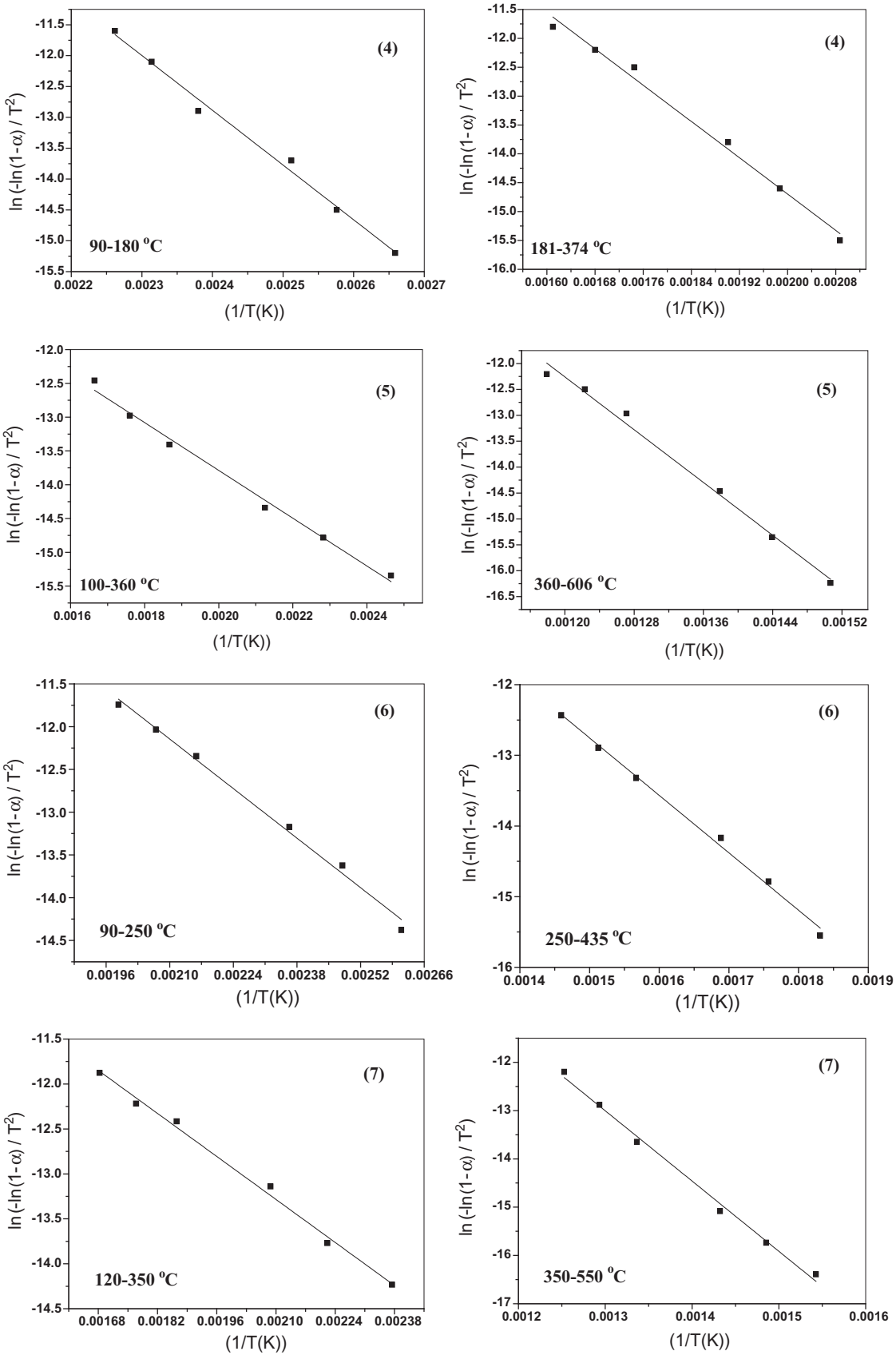

Fig. 10 (*continued*)

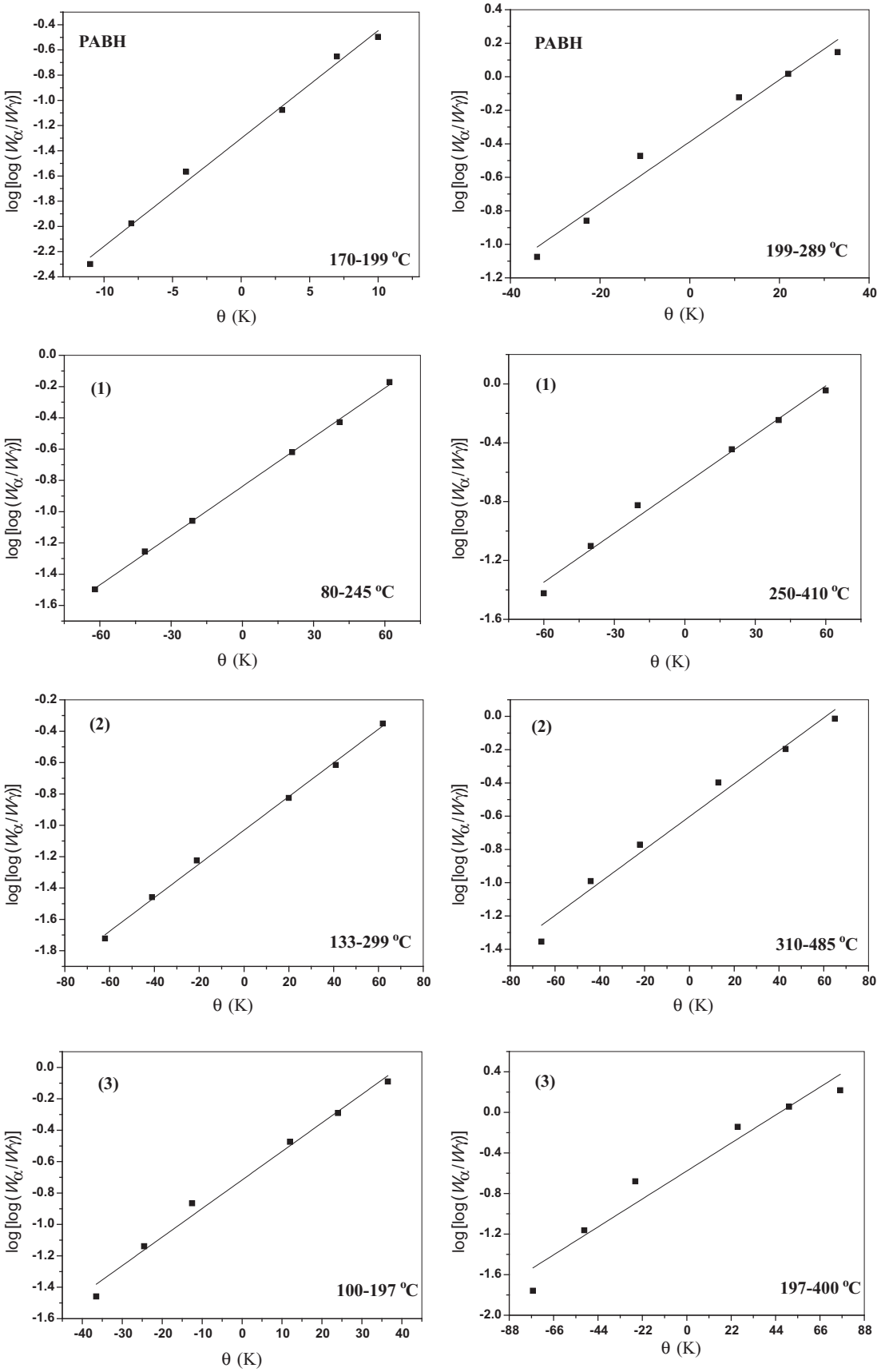

Fig. 11. Horowitz–Metzger (HM) of PABH homopolymer and its polymer complexes (**1**–**7**).

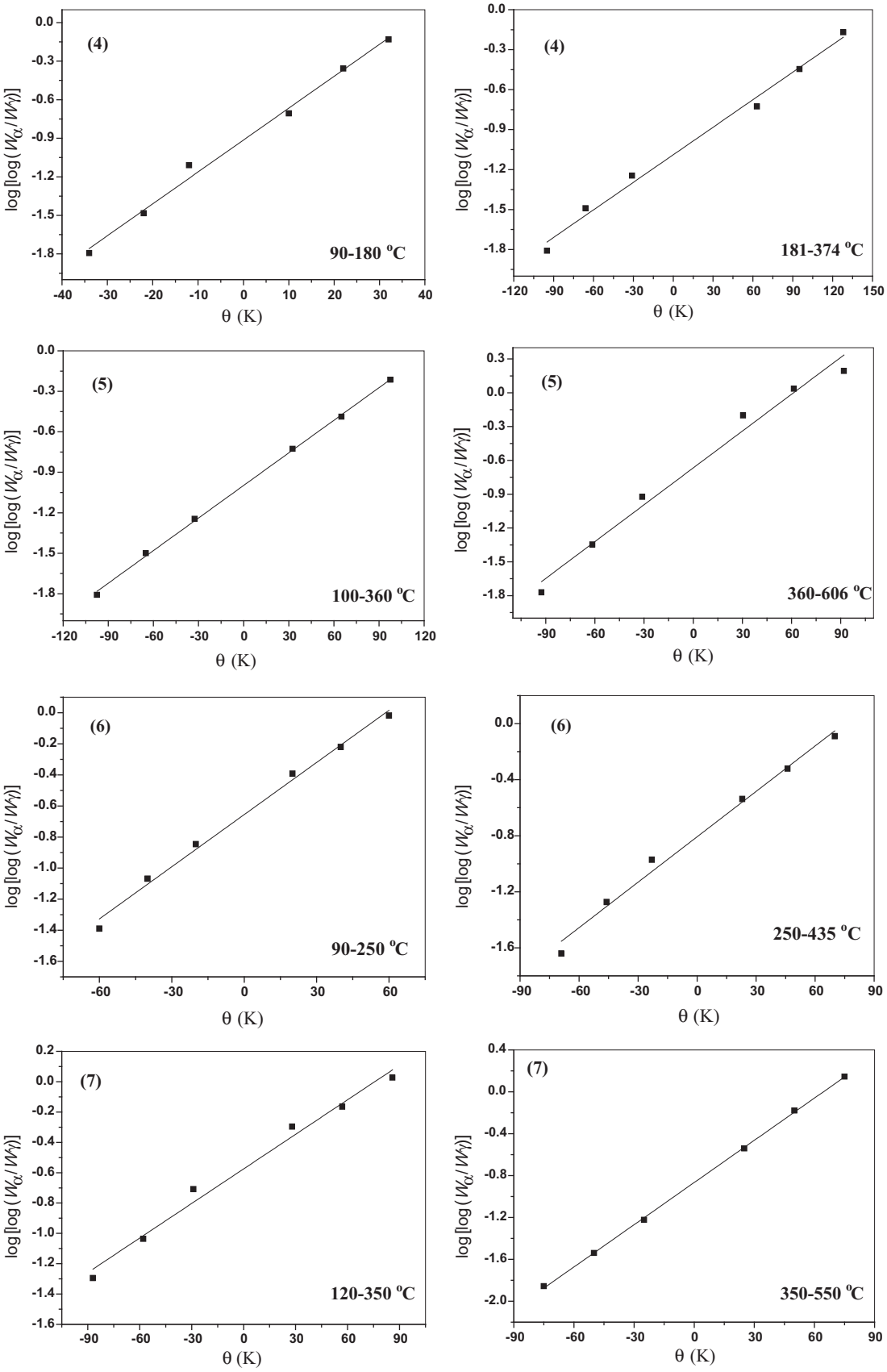

Fig. 11 (*continued*)

Table 8
Thermodynamic activation energy for PABH homopolymer and its polymer complexes (**1–7**).

Compound[a]	Temp. range (°C)	Method	Parameter				
			E_a (kJ mol^{-1})	A (s^{-1})	ΔS^* (J mol^{-1} K^{-1})	ΔH^* (kJ mol^{-1})	ΔG^* (kJ mol^{-1})
PABH	170–199	CR	341	2.58E+36	4.49E+02	337	131
		HM	344	5.17E+37	4.74E+02	340	123
	199–289	CR	84.6	2.27E+06	−1.28E+02	80.3	146
		HM	94.5	2.50E+07	−1.08E+02	90.2	146
1	80–245	CR	30.8	5.80E+00	−2.33E+02	27.2	129
		HM	38.1	1.50E+02	−2.06E+02	34.5	124
	250–410	CR	67.0	1.21E+03	−1.92E+02	62.0	178
		HM	77.5	2.18E+04	−1.68E+02	72.4	174
2	133–299	CR	40.0	1.51E+01	−2.26E+02	36	147
		HM	49.2	7.41E+02	−1.94E+02	45.1	140
	310–485	CR	73.1	1.00E+03	−1.94E+02	67.5	198
		HM	85.1	1.64E+04	−1.71E+02	79.6	194
3	100–197	CR	54.7	1.73E+04	−1.67E+02	51.2	121
		HM	61.9	3.27E+05	−1.42E+02	58.4	118
	197–400	CR	68.7	5.57E+03	−1.79E+02	63.9	166
		HM	78.4	7.02E+04	−1.58E+02	73.7	164
4	90–180	CR	73.8	6.65E+06	−1.17E+02	70.4	118
		HM	79.9	1.45E+08	−9.13E+01	76.5	114
	181–374	CR	65.3	3.63E+03	−1.82E+02	60.8	161
		HM	75.2	6.82E+04	−1.57E+02	70.6	157
5	100–360	CR	29.4	7.15E−01	−2.52E+02	25.2	152
		HM	39.0	3.48E+01	−2.20E+02	34.8	145
	360–606	CR	106	4.35E+04	−1.64E+02	99.6	223
		HM	119	7.33E+05	−1.40E+02	113	219
6	90–250	CR	34.4	2.19E+01	−2.23E+02	30.7	129
		HM	42.1	3.91E+0	−1.99E+02	38.4	126
	250–435	CR	67.6	7.74E+02	−1.96E+02	62.5	183
		HM	78.3	1.83E+04	−1.69E+02	73.1	177
7	120–350	CR	28.4	1.27E+00	−2.47E+02	24.2	150
		HM	37.6	2.13E+01	−2.24E+02	33.4	147
	350–550	CR	121	9.02E+05	−1.38E+02	115	215
		HM	135	2.71E+07	−1.10E+02	129	208

[a] The number corresponds to that used in Table 1.

[53] Accordingly, if $G < 4$, then the exchange interaction may be present, if $G > 4$, then the exchange interaction may be negligible; however, which is the case in the polymer complexes under investigation. Interestingly, in these complexes, $G > 4$, suggesting the presence of an exchange interaction may be negligible. The magnetic moments of these polymer complexes are normal at room temperature. The G values follow the order:

$$\left[[Cu(AB)(ONO_2)(OH_2)]\cdot\frac{3}{4}H_2O\right]_n > \left[[Cu(AB)_2]\cdot\frac{5}{4}H_2O\right]_n > \left[[Cu(AB)(OAc)]\cdot\frac{1}{2}H_2O\right]_n > \left[[Cu(ABH)(O_2SO_2)]\cdot\frac{3}{4}H_2O\right]_n.$$

This is consistent with the order of the strength of metal–anion interactions, i.e. nitrate > acetate > sulfate. Our results are also in agreement with the respective positions of these anions as given in the representative Pascal constants [46].

$A_{||}$ polymer complexes exhibit $g_{||} < 2.3$, suggesting covalent characters of the copper–ligand bonding in the present polymer complexes. The $g_{||}/A_{||}$ is taken as an indication for the stereochemistry of the copper(II) polymer complexes. Addison has suggested that this ratio may be an empirical indication of the tetrahedral distortion of the square planar geometry [54]. The values lower than 135 cm^{-1} are observed for square planar structures and those higher than 150 cm^{-1} for tetrahedrally distorted complexes. The values for the polymer complexes under investigation. Table 9, showed that all polymer complexes associated with a square planar ligand around the copper(II) centers. The $g_{||}/A_{||}$ values lie just within the range expected for the complexes.

The g-values of the copper(II) polymer complexes with a $^2B_{1g}$ ground state ($g_{||} > g_{\perp}$) may be expressed [55] by:

$$g_{||} = 2.0023 - (8K_{||}^2\lambda_0/\Delta E_{xy})$$

$$g_{\perp} = 2.0023 - (2K_{\perp}^2\lambda_0/\Delta E_{xz})$$

Table 9
ESR spectral and calculated bonding parameters for the Cu(II) complexes (**2–5**).

Complex[a]	$g_{||}$	$g_{\perp}$	$g_{av.}$	G	α^2	$A_{||}$[b]	$g_{||}/A_{||}$[c]	ΔE_{xy} (cm^{-1})	ΔE_{xz} (cm^{-1})	$K_{\perp}^2$	$K_{||}^2$	K^2	β^2	β_1^2
2	2.246	2.057	2.120	4.32	0.80	177	127	18310	19810	0.685	0.675	0.67	0.82	0.84
3	2.260	2.045	2.117	5.78	0.93	221	102	18590	20215	0.525	0.724	0.60	0.56	0.78
4	2.258	2.061	2.127	4.20	0.90	196	115	18570	20195	0.719	0.720	0.72	0.80	0.80
5	2.250	2.060	2.123	4.17	0.84	167	134	18550	20090	0.695	0.700	0.70	0.84	0.83

[a] The number corresponds to that used in Table 1.
[b] A values in 10^{-4} (cm^{-1}).
[c] The unit (cm^{-1}).

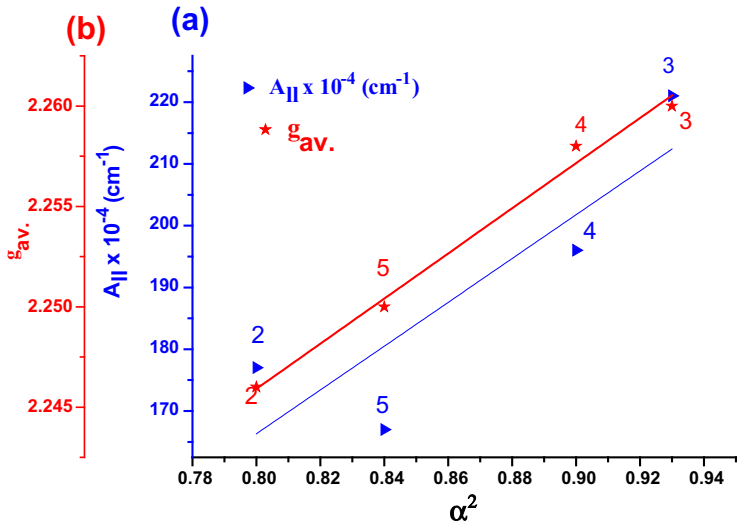

Fig. 12. The relation between α^2 vs. (a) $A_{||} \times 10^{-4}$ (cm^{-1}) and (b) $g_{av.}$

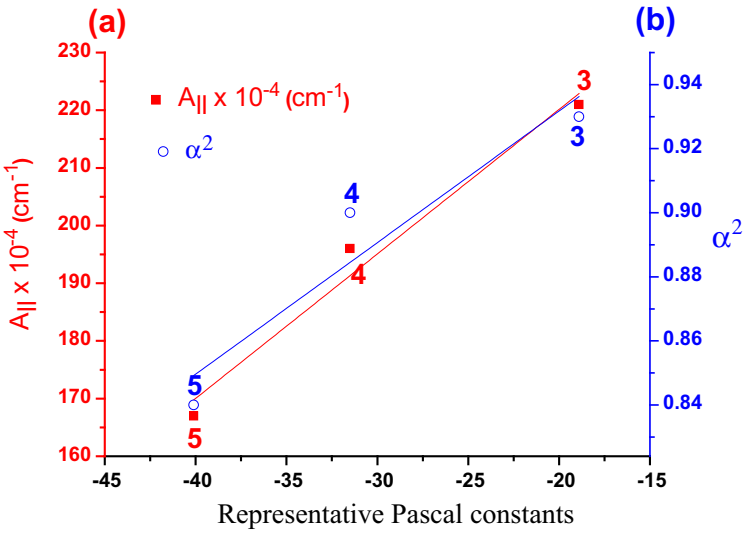

Fig. 13. The relation between representative Pascal constants of complexes (**3**–**5**) and (a) $A_{||} \times 10^{-4}$ (cm^{-1}) and (b) α^2.

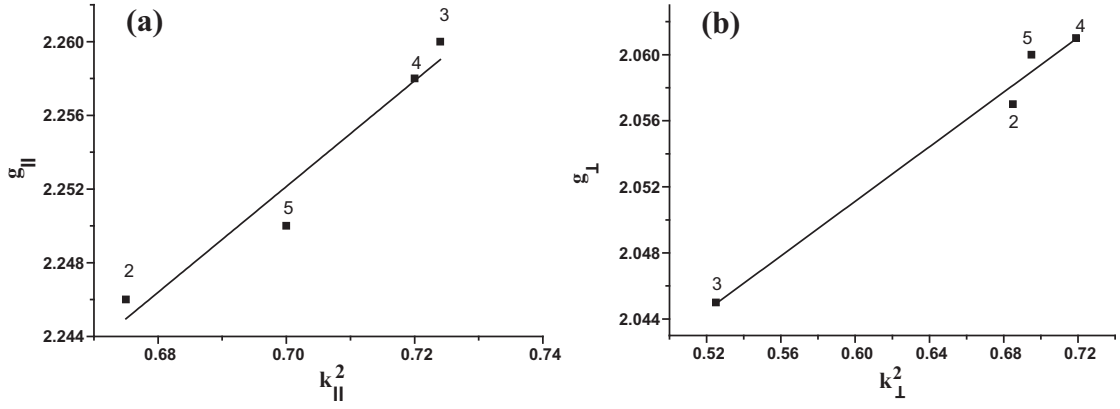

Fig. 14. The relation between (a) $K_{||}^2$ vs. $g_{||}$ and (b) $K_\perp^2$ vs. $g_\perp$.

where $K_{||}$ and $K_\perp$ are the parallel and perpendicular components respectively of the orbital reduction factor (K), λ_0 is the spin–orbit coupling constant for the free copper, ΔE_{xy} and ΔE_{xz} are the electron transition energies of $^2B_{1g} \rightarrow {}^2B_{1g}$ and $^2B_{1g} \rightarrow {}^2E_g$ From the above relations, the orbital reduction factor ($K_{||}$, $K_\perp$, K), which are a measure of covalency [55], can be calculated. For an ionic environ-

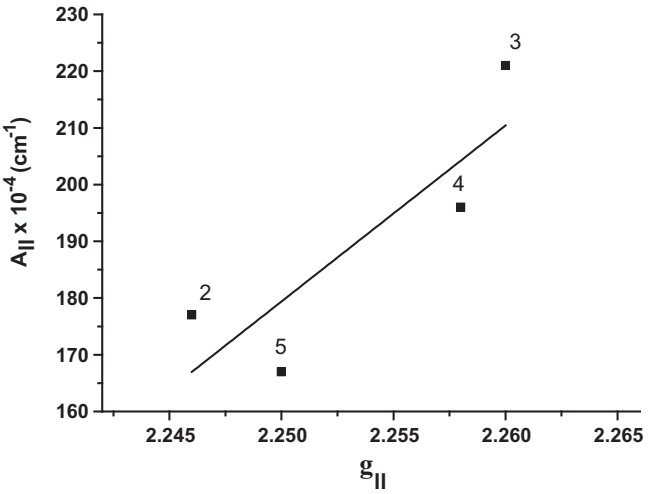

Fig. 15. The relation between $g_{||}$ vs. $A_{||} \times 10^{-4}$ (cm^{-1}).

ment, $K = 1$ and for a covalent environment $K < 1$, the lower value of K, the greater is the covalency.

$$K_{\perp}^2 = (g_{\perp} - 2.0023)\Delta E_{xz}/2\lambda_0$$

$$K_{||}^2 = (g_{||} - 2.0023)\Delta E_{xy}/8\lambda_0$$

$$K^2 = (K_{||}^2 + K_{\perp}^2)/3$$

The K values (Table 9) for the copper(II) polymer complexes are indicative of their covalent nature [56]. Kivelson and Neiman [22] noted that, for an ionic environment, $g_{||} \geqslant 2.3$. Theoretical work by Smith [57] seems to confirm this view. The $g_{||}$-values reported here show considerable covalent bonding character. Also, the in-plane σ-covalency parameter α^2 was calculated. The calculated values (Table 9) suggest covalent bonding nature [58].

The in-plane and out-of-plane π-bonding coefficient (β_1^2 and β, respectively) are dependent upon the values of ΔE_{xy} and ΔE_{xz} in the following equations [58]:

$$\alpha^2\beta^2 = (g_{\perp} - 2.0023)\Delta E_{xz}/2\lambda_0$$

$$\alpha^2\beta_1^2 = (g_{||} - 2.0023)\Delta E_{xy}/8\lambda_0$$

In this work, the polymer complexes show β_1^2 values 0.78–0.84 indicating a moderate degree of covalency in the in-plane π-bonding, while β^2 are 0.56–0.82 indicating ionic and covalent character of the out-of-plane π-bonding. These ESR data showed that:

(i) $g_{||}$ values are dependent on the nature of the co-coordinated ligand and the ordered as: $NO_3^- > OAc^- > SO_4^{2-}$ which in agreement with the electronic spectral data. The reverse order is observed for $A_{||}$.
(ii) The value of α^2 increases with increasing $g_{av.}$ and $A_{||}$ as shown in Fig. 12.
(iii) The value of Pascal constants of complexes increases with increasing $A_{||}$ and α^2 as shown in Fig. 13.
(iv) $K_{||}^2$ and $K_{\perp}^2$ increase with increasing $g_{||}$ and $g_{\perp}$ as shown in Fig. 14.
(v) β_1^2 increase with decreasing $g_{||}$.

The above results shows clearly the effect of halogen groups on the ESR parameter on the stereochemistry of copper(II) polymer complexes. It is important to note that the existence of halogen groups enhances the electron density on the coordination sites and simultaneously increase the value of ESR parameters (Table 9).

The plot of $A_{||}$ vs. $g_{||}$ (Fig. 15) shows a linear relationship between $A_{||}$ and $g_{||}$ for each chromophore. The $A_{||}$ and $g_{||}$ values are relatively insensitive to the inductive effect of the co-ligand and chiefly depend on the stereochemical factors. The $g_{||}$ values are weaker in the "O,O" compounds in agreement with the more electron donating character of the nitrogen atom.

Conclusion

The structures of the Cu(II), Co(II), Ni(II) and UO_2(II) ions polymer complexes of ABH were confirmed by elemental analyses, IR, ^{1}H NMR, molar conductance and thermal analysis data. Therefore, from IR spectrum, it is concluded that ABH binds to the metal ions through protonated carboxylate O and phenolic OH [except complex (**5**)]. Three types of polymeric complexes were prepared. In type [(**1**) & (**2**)](1:2) (monobasic and bis-bidentate) the chelate rings are six-membered/four coordinate, whereas in type [(**3**) & (**4**)](1:1) (monobasic and bidentate) they are six-membered/four coordinate, monobasic and bidentate. In type [5](1:1) (neutral and bidentate) the chelate is six-membered/four coordinate. While in case of complex (**5**), it coordinates *via* its COOH/OH. From the molar conductance, it is found that all polymer complexes are non-electrolytes. The ^{1}H NMR spectra of ABH and its UO_2(II) polymer complex show that the COOH signal in the free ligand is completely disappeared in the spectrum of the UO_2(II) polymer complex indicating the involvement of the COOH group in chelation through displacement of the COOH proton. The values of activation energies of decomposition (E^*) are found to be 341.46, 36.87, 47.58, 79.81, 77.58, 35.70, 41.93 and 34.46 kJ/mol for PABH and its polymer complexes (**1**–**7**), respectively. It is clear that, the activation energy of PABH is greatly higher than its polymer complexes (**1**–**7**).

References

[1] M. Karabacak, M. Kurt, J. Mol. Struct. 919 (2009) 215–222.
[2] M. Karabacak, E. Kose, M. Kurt, J. Raman Spectrosc. 41 (2010) 1085–1097.
[3] M. Takahashi, Y. Ishikawa, H. Ito, Chem. Phys. Lett. 531 (2012) 98–104.
[4] P. Wen, J. Chen, S. Wan, W. Kong, P. Zhang, W. Wang, J. Zhan, Q. Pan, W. Huang, Plant Growth Regul. 55 (2008) 1–10.
[5] F. Hasanain, Z.Y. Wang, Polymer 49 (2008) 831–835.
[6] S. Zaugg, X. Zhang, J. Sweedler, W. Thormann, J. Chromatogr. B Biomed. Sci. Appl. 752 (2001) 17–31.
[7] O.I. Aruoma, Free Radic. Biol. Med. 20 (1996) 675–705.
[8] C.A. Rice-Evans, N.J. Miller, G. Paganga, Free Radic. Biol. Med. 20 (1996) 933–956.
[9] U. Nagashima, S. Nagaoka, S. Katsumata, J. Phys. Chem. 95 (1991) 3532–3538.
[10] C. Elvira, J. San Román, Polymer 38 (1997) 4743–4750.
[11] K.S. Khairou, M.A. Diab, Polym. Degrad. Stab. 43 (1994) 329–333.
[12] M.M. Ghoneim, N.A. El-Ghamaz, A.Z. El-Sonbati, M.A. Diab, A.A. El-Bindary, L.S. Serag, Spectrochim. Acta A 137 (2015) 1039–1049.
[13] A.A. El-Bindary, A.Z. El-Sonbati, M.A. Diab, M.E. Attallah, Spectrochim. Acta A 86 (2012) 547–553.
[14] M.A. Diab, A.Z. El-Sonbati, R.H. Mohamed, Spectrochim. Acta A 77 (2010) 795–801.
[15] N.A. El-Ghamaz, M.A. Diab, A.A. El-Bindary, A.Z. El-Sonbati, H.A. Seyam, Mater. Sci. Semicond. Process. 27 (2014) 521–531.
[16] A.A. El-Bindary, A.Z. El-Sonbati, M.A. Diab, E.E. El-Katori, H.A. Seyam, Int. J. Adv. Res. 2 (2014) 493–502.
[17] G. Gao, C. Liang, Electrochim. Acta 52 (2007) 4554–4559.
[18] Y. Feng, S. Chen, W. Guo, Y. Zhang, G. Liu, J. Electroanal. Chem. 602 (2007) 115–122.
[19] N.A. El-Ghamaz, A.Z. El-Sonbati, M.A. Diab, A.A. El-Bindary, M.K. Awad, Sh.M. Morgan, Mater. Sci. Semicond. Process. 19 (2014) 150–162.
[20] P. Geerlings, F. De Proft, W. Langenaeker, Chem. Rev. 103 (2003) 1793–1873.
[21] P.K. Chattaraj, S. Giri, J. Phys. Chem. A 111 (2007) 11116–11121.
[22] D. Kivelson, R. Niemen, J. Chem. Phys. 35 (1961) 149–155.
[23] M. Boczar, Ł. Boda, M.J. Wòjcik, Spectrochim. Acta A 64 (2006) 757–760.
[24] A. Syamal, M.R. Maurya, Coord. Chem. Rev. 95 (1989) 183–238.
[25] M.H. Soliman, G.G. Mohamed, Spectrochim. Acta A 107 (2013) 8–15.

[26] A.Z. El-Sonbati, M.A. Diab, A.A. El-Bindary, Stoichiometry and Research the Importance of Quantity in Biomedicine, Pub. by In Tech, Janeza Trdine 9, 51000 Rijeka, Croatia. P. Cm ISBN 978-953-51-0198-7, 2012 (Chap. 7), pp. 147–194.
[27] C. Gorller-Walrand, S.D.E. Jeogere, Spectrochim. Acta A 28 (1972) 257–268.
[28] G.K. Sandhu, S.P. Verma, Polyhedron 6 (1987) 587–591.
[29] M.A. Diab, A.A. El-Bindary, A.Z. El-Sonbati, O.L. Salem, J. Mol. Struct. 1018 (2012) 176–184.
[30] S.K. Jain, B.S. Garg, Y.K. Bhoon, Spectrochim. Acta A 42 (1986) 701–737.
[31] K. Nakamoto, Infrared and Raman Spectra of Inorganic and Coordination Compounds, fifth ed., Wiley, New York, 1997.
[32] A.Z. El-Sonbati, M.A. Diab, A.A. El-Bindary, Sh.M. Morgan, Spectrochim. Acta A 127 (2014) 310–328.
[33] A.Z. El-Sonbati, M.A. Diab, A.A. El-Bindary, A.M. Eldesoky, Sh.M. Morgan, Spectrochim. Acta A 135 (2015) 774–791.
[34] M.A. Diab, A.A. El-Bindary, A.Z. El-Sonbati, O.L. Salem, J. Mol. Struct. 1007 (2012) 11–19.
[35] S.P. McGlynn, J.K. Smith, W.C. Neely, J. Chem. Phys. 35 (1961) 105.
[36] M.M. Ghoneim, A.Z. El-Sonbati, M.A. Diab, A.A. El-Bindary, L.S. Serag, J. Polym. Plast. Technol. Eng. 54 (2015) 100–117.
[37] L.H. Jones, Spectrochim. Acta A 11 (1959) 409–411.
[38] A.Z. El-Sonbati, M.A. Diab, A.A. El-Bindary, Sh.M. Morgan, Inorg. Chim. Acta 404 (2013) 175–187.
[39] S. Basavaraja, D.S. Balaji, M.D. Bedre, D. Raghunandan, P.M.P. Swamy, A. Venkataraman, Bull. Mater. Sci. 34 (2011) 1313–1317.
[40] M.I. Abd-Elrahman, R.M. Khafagy, Sh.A. Zaki, M.M. Hafiz, Mater. Sci. Semicond. Process. 18 (2014) 1–5.
[41] S. Velumani, X. Mathew, P.J. Sebastian, Sol. Energy Mater. Sol. Cells 76 (2003) 359–368.
[42] B. Saifullah, M.Z. Hussein, S.H. Hussein-Al-Ali, P. Arulselvan, S. Fakurazi, Chem. Cent. J. 7 (2013) 72–82.
[43] M.K. Rotich, B.D. Glass, M.E. Brown, J. Therm. Anal. Calorim. 64 (2001) 681–688.
[44] M.A. Diab, A.Z. El-Sonbati, A.A. El-Bindary, A.M. Barakat, Spectrochim. Acta A 116 (2013) 428–439.
[45] M.A. Diab, A.Z. El-Sonbati, D.M.D. Bader, Spectrochim. Acta A 79 (2011) 1057–1062.
[46] A.B.P. Lever, E. Mantovani, Inorg. Chem. 10 (1971) 817–826.
[47] A.W. Coats, J.P. Redfern, Nature 20 (1964) 68–79.
[48] H.W. Horowitz, G. Metzger, Anal. Chem. 35 (1963) 1464–1468.
[49] M. Odabasoglu, F. Arslan, H. Olmmez, O. Buyukgungor, Dyes Pigments 75 (2007) 507–515.
[50] Z. Chen, Y. Wu, D. Gu, F. Gan, Spectrochim. Acta A 68 (2007) 918–926.
[51] A.Z. El-Sonbati, A.A. El-Bindary, M.A. Diab, S.G. Nozha, Spectrochim. Acta A 83 (2011) 490–498.
[52] H.A. Kuska, M.T. Rogers, in: A.E. Marcell (Ed.), Coordination Chemistry, Van Nostrand Reinhold Co, NY, 1971.
[53] I.M. Procher, B.J. Hathaway, P. Nichoils, J. Chem. Soc. A (1968) 1678–1684.
[54] U. Sakaguchi, A.W. Addison, J. Chem. Soc., Dalton Trans. (1979) 600–608.
[55] A.Z. El-Sonbati, A.A. El-Bindary, S.M. Mabrouk, R.M. Ahmed, Spectrochim. Acta A 57 (2001) 1751–1757.
[56] A.E. El-Sonbati, M.A. Diab, Physico-chemical Studies on the Complexes, LA LAMBERT Academic Publishing GmbH, Leipzig & Co., KG, Germany, 2010 (ISBN: 978-3-8433-7229-9).
[57] D.W. Smith, J. Chem. Soc. A (1970) 3108–3120.
[58] B.J. Hathaway, G. Wilkinson, R.D. Gihard, J.A. McGleverty (Eds.), Comprehensive Coordination Chemistry II, vol. 5, Pergamon, Oxford, 1987.